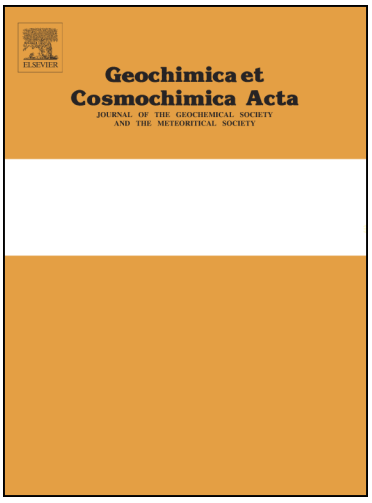

Reconstructing carbonate alteration histories in orogenic sedimentary basins: Xigaze forearc, southern Tibet

Miquela Ingalls

PII: S0016-7037(19)30082-1
DOI: https://doi.org/10.1016/j.gca.2019.02.005
Reference: GCA 11120

To appear in: *Geochimica et Cosmochimica Acta*

Received Date: 28 July 2018
Accepted Date: 4 February 2019

Please cite this article as: Ingalls, M., Reconstructing carbonate alteration histories in orogenic sedimentary basins: Xigaze forearc, southern Tibet, *Geochimica et Cosmochimica Acta* (2019), doi: https://doi.org/10.1016/j.gca.2019.02.005

Reconstructing carbonate alteration histories in orogenic sedimentary basins: Xigaze forearc, southern Tibet

Miquela Ingalls[a,b,*]

[a] *Division of Geological and Planetary Sciences, California Institute of Technology, Pasadena, CA*
[b] *Department of Geological Sciences, University of Colorado, Boulder, CO*

Abstract

Carbonate clumped isotope thermometry ($T(\Delta_{47})$) and the oxygen stable isotope record ($\delta^{18}O$) provide critical constraints on the temperature of carbonate mineral formation and isotopic composition of ancient waters used in reconstructions of past climate, tectonics, and ecological and environmental change. The robust use of these proxies requires that carbonate minerals in the rock record retain primary isotopic compositions through often complex post-depositional thermal histories. New carbonate clumped isotope thermometry and sedimentology data are paired with existing thermochronology and isotope exchange reaction modeling to provide unique constraints on the alteration history of the carbon and oxygen isotopes in Tethyan marine carbonates (Jialazi Fm, Tso Jianding Group) of the Xigaze forearc, southern Tibet. Within the framework of the textural and isotopic data, the effects of early and late burial alteration on Δ_{47} and $\delta^{18}O$ values of marine rocks that were buried to <6 km and uplifted to >4 km above sea level are modeled. The alteration products are considered within two well-studied mechanistic frameworks: water-rock recrystallization and solid-state reordering of ^{13}C-^{18}O bonds at high temperature. The proposed alteration model is as follows: (1) shallow, early diagenesis with water of similar composition and temperature to formation waters infills primary porespace with

*Corresponding author
Email address: mingalls@caltech.edu (Miquela Ingalls)

microspar; (2) high-temperature, rock-buffered water-rock exchange and partial solid-state reordering at >3-4 km depth; and (3) near-surface, low-temperature water-rock exchange on the exhumation pathway. The Δ_{47} heterogeneity within individual samples (0.456 to 0.721) requires significant differential alteration on the retrograde path (high to low temperature, low water-rock ratio) in which primary compositions and compositions inherited during early burial diagenesis are overprinted with modern meteoric values. A low T(Δ_{47}) value is often assumed to record the primary temperature of the depositional environment. However, samples yielding low T(Δ_{47}) values in the Jialazi Fm have undergone extensive high-temperature water-rock alteration, and therefore, require a mechanism for increasing ^{13}C-^{18}O bond ordering on the retrograde pathway while preserving many primary biogenic structures and micritic textures. This study highlights the potential significance of late-stage, low-temperature alteration of carbonates derived from orogenic sedimentary basins for studies of terrestrial paleoenvironments and tectonics. This study also provides an example framework for combining observational and analytical data to reconstruct a carbonate alteration history of a buried sedimentary package.

Keywords: carbonate alteration, clumped isotope thermometry, burial diagenesis, proxy assessment, water-rock alteration

1. Introduction

Carbonate 'clumped' isotope (Δ_{47}) thermometry is based on the predictable degree of multiple isotope substitution—'clumping' of the rare isotopes, ^{13}C and ^{18}O, within the carbonate (CO_3^{2-}) lattice—at distinct formation temperatures relative to a random distribution of ^{13}C and ^{18}O within the same carbonate group (Eiler, 2007). The thermodynamic relationship between ^{13}C-^{18}O bond ordering and temperature relies only on the homogeneous equilibrium between carbonate ions, and therefore provides a means to reconstruct past mineral formation temperatures (T(Δ_{47})) without independent knowledge of the oxygen isotopic composition of formation water ($\delta^{18}O_w$). This critical difference

between the Δ_{47} and $\delta^{18}O$ thermometers has advanced the field of carbonate diagenesis by enabling calculation of diagenetic paleofluid compositions and sources, and refining thermal histories of faulted and buried sedimentary basins (Bergman et al., 2013; Dale et al., 2014; Swart et al., 2016; Faÿ-Gomord et al., 2018; Mangenot et al., 2018).

T(Δ_{47}) was originally developed as an important tool for reconstructing ancient climates (Eiler, 2007, 2011; Keating-Bitonti et al., 2011; VanDeVelde et al., 2013; Snell et al., 2013), tectonics (Ghosh et al., 2006b; Snell et al., 2014; Huntington et al., 2015; Ingalls et al., 2017b), terrestrial and marine environments (Passey et al., 2010; Zaarur et al., 2011), and ecology (Eagle et al., 2010; Henkes et al., 2013). Determining past Earth surface conditions requires that the carbonate mineral remains unaltered through all post-depositional events. However, the carbonates are often sampled from orogenic sedimentary basins with complex thermal histories. Therefore, it is essential to develop tools to better understand the thermal histories of paleoenvironmental proxies, and to critically assess textural and isotopic alteration after original mineral formation.

The degree of isotopic 'clumping' can be altered in two ways: (i) water-facilitated recrystallization, and (ii) solid-state reordering of carbon-oxygen (C–O) bonds within the carbonate crystal lattice at temperatures >∼75°C for tens of millions of years (Passey and Henkes, 2012; Henkes et al., 2014; Stolper and Eiler, 2015). Within this framework, and enabled by carbonate oxygen isotope ($\delta^{18}O_c$) and Δ_{47} measurements, this work builds a carbonate alteration history for the Jialazi Formation (Xigaze forearc, southern Tibet), which records a critical transition from shallow marine to terrestrial deposition during the early stages of India-Asia collision (Orme et al., 2014). Late Paleocene-early Eocene, low-latitude marine carbonate should yield $\delta^{18}O_c$ of ∼–2 to –3 ‰ VPDB (Kobashi et al., 2001) and formation temperatures of ∼25 to 30°C. However, in the ∼60 My since shallow marine deposition, the Jialazi Fm has been buried >6 km with an opportunity to interact with non-marine diagenetic fluids along the burial-exhumation pathway. In addition, the Jialazi Fm currently interacts with extremely low $\delta^{18}O_w$ meteoric water >4 km above sea level on

the Tibetan Plateau (Bershaw et al., 2012). The marine samples in this work are geologically and isotopically ideal for investigating mechanisms and isotopic effects of carbonate burial diagenesis because (1) the initial isotopic values are constrained by known marine compositions and low-latitude sea surface temperatures (Kobashi et al., 2001; Miller et al., 1987; Ivany et al., 2003), and starkly contrast $\delta^{18}O_w$ of modern Tibetan meteoric water, and (2) apatite and zircon (U-Th)/He (AHe; ZHe) thermochronometry provide constraints on the burial history of these strata ($\sim$160 to $>$200°C; Orme (2017)).

In this work, water-rock and solid-state isotope exchange reaction modeling is performed within the time-temperature framework of the AHe and ZHe time-temperature history (Orme, 2017). Next, the results of the modeling exercises are synthesized with $\delta^{18}O_c$ and Δ_{47} measurements, constraints on the starting $\delta^{18}O$ composition of shallow marine carbonate and early Cenozoic low-latitude sea surface temperature (Kobashi et al., 2001; Miller et al., 1987; Ivany et al., 2003), and physical assessment of the carbonate morphologies and fabrics from optical and cathodoluminescence petrography to (1) refine our understanding of the alteration history of carbonates from the Jialazi Fm of the Xigaze forearc, (2) develop a broader, mechanistic understanding of carbonate alteration within active orogenies and tectonic settings, and (3) provide new insight into how paired measurements and models from orogenic sedimentary basins can be used to better understand regional tectonics.

1.1. Water-rock isotopic exchange during carbonate recrystallization

Carbonate recrystallization typically occurs by dissolution-precipitation reactions driven by geochemical disequilibria between minerals and fluids. The extent to which $\delta^{18}O_w$ and $\delta^{18}O_c$ isotopically converge depends largely on the water-rock ratio (W:R), porosity, temperature, and open- versus closed-system behavior (Banner and Hanson, 1990). No matter the W:R of a system, carbonate and fluid will exchange until either chemical equilibrium is reached, or the water is removed from the system.

Recrystallized carbonate should record a relative mixture of the stable iso-

topic compositions of the original carbonate and the diagenetic carbonate precipitated in equilibrium with the alteration fluid. In creating new carbonate material, dissolution-precipitation also creates new C–O bonds, thereby altering Δ_{47}. The Δ_{47} value of a recrystallized mineral records a non-linear mixture of the primary and secondary components (Defliese and Lohmann, 2015). Δ_{47} does not appreciably alter during shallow burial (<1 km) because the difference between depositional and buried T(Δ_{47}) is relatively insignificant (Stolper et al., 2018).

1.2. Solid-state reordering during deep burial

When carbonate is exposed to elevated temperatures (e.g. due to proximity to magmatic intrusions or deep burial), the original C–O bonds within the crystal lattice reorder without recrystallization (Stolper and Eiler, 2015; Ghosh et al., 2006a; Dennis and Schrag, 2010). Solid-state reordering overprints the primary mineral formation Δ_{47} and T(Δ_{47}), initially as partial reordering and trending towards equilibrium in elevated (>150°C) temperature regimes (Passey and Henkes, 2012; Henkes et al., 2014). In recent years, the kinetics of these closed-system isotope exchange reactions have been constrained by measurements of natural carbonatites (Dennis and Schrag, 2010) and marbles (Ghosh et al., 2006a), laboratory heating experiments (Lloyd et al., 2018), and modeling efforts (Passey and Henkes, 2012; Henkes et al., 2014; Stolper and Eiler, 2015). These models have explored kinetic parameters related to material type (Passey and Henkes, 2012; Henkes et al., 2014; Lloyd et al., 2018), differing burial-exhumation histories (Shenton et al., 2015), diffusion of isotopes through the crystal lattice and isotope-exchange reactions between adjacent carbonate groups (Stolper and Eiler, 2015).

Stolper and Eiler (2015) demonstrated that natural carbonates undergo Δ_{47} alteration in two temperature-dependent stages. Under a lower temperature regime (∼75 to <150°C), there is rapid exchange between neighboring carbonate groups within the crystal lattice that each contain one rare isotope, and the measured T(Δ_{47}) is never in equilibrium with the ambient temperature. For ex-

ample, a carbonate rock held at 75°C for 100 million years will experience <1°C increase in T(Δ_{47}), but the T(Δ_{47}) of the same carbonate held at 120°C will increase by up to 40°C. The second stage requires a slower process of diffusion of ^{13}C and ^{18}O away from each other through the crystal lattice, yielding lower Δ_{47} values. At temperatures above 150°C, the kinetics are sufficient for the apparent equilibrium T(Δ_{47}) temperature to catch up to the true temperature of the burial setting.

Solid-state exchange reactions almost invariably lead to lower Δ_{47} values due to scrambling of the clumped species (^{13}C-^{18}O), but calcite can partially reorder to higher Δ_{47} values on the retrograde path when the rate of cooling exceeds the thermodynamic impetus for C–O bonds to remain isotopically disordered (Passey and Henkes, 2012; Stolper and Eiler, 2015). The final recorded temperature is referred to as the "apparent equilibrium blocking temperature" (Stolper and Eiler, 2015), which forms a time-temperature plateau. Greater ^{13}C-^{18}O ordering cannot be restored to original Earth surface values in the solid-state on geologic timescales, and Δ_{47} only appreciably increases via recrystallization at lower temperature. Reaction kinetics are slower at lower temperatures, and thus recrystallization at surface temperatures proceeds slowly; as a result, a high Δ_{47} value is often assumed to record primary (low-T) carbonate formation conditions. However, if carbonate δ^{18}O and Δ_{47} can be altered by recrystallization at low temperatures in an exhumed sedimentary package without petrographic evidence of significant recrystallization, then prior low T(Δ_{47}) measurements from ancient, buried carbonates would need to be reconsidered as evidence of primary Earth surface conditions. Evidence of such reordering mechanisms is explored in this work.

2. Geologic Setting

2.1. Xigaze forearc basin

The stratigraphy of the Xigaze forearc basin records Cretaceous to lower Eocene sedimentation along the southern margin of the Lhasa block (Einsele

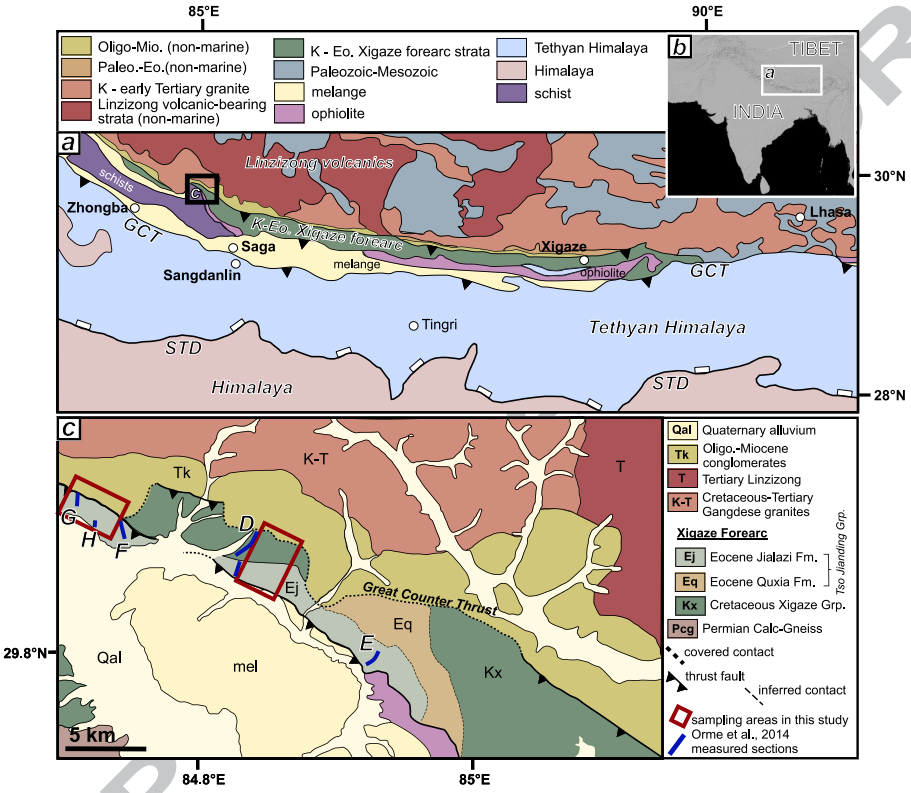

Figure 1: **Map of Xigaze forearc strata in study area adapted from Orme et al. (2014). A.** Regional geology of northern India and southern Tibet in the Xigaze forearc region. The black square marks the location of the study region. **b.** Location map. **B.** Cretaceous to Eocene Xigaze forearc strata are bounded by the north-vergent Great Counter Thrust system. The navy blue lines indicate measured stratigraphic sections from Orme et al. (2014); the maroon boxes indicate measured and sampled sections from this study.

et al., 1994; Wan et al., 1998; Ding et al., 2005; Wang et al., 2011, 2012; Bouilhol et al., 2013; Orme et al., 2014; Carrapa et al., 2014; Hu et al., 2015; Leary et al., 2016; Orme and Laskowski, 2016; Hu et al., 2016), and thus, provides an exceptional opportunity to study the evolving geology of Asia's southern margin prior to and through the earliest stage of collision. The initial collision is marked by the arrival of distinctly Asian sediments overlying and interbedded with Indian sediments by at least 58±2 Ma (DeCelles et al., 2014). Due to the asymmetric topography of the Indian and Eurasian plates at the time of collision—a marine shelf and a high elevation magmatic arc, respectively—the detrital sedimentary record of collisional onset is located on the lower, Indian plate (DeCelles et al., 2014).

The preserved Xigaze forearc basin stratigraphy, which sits today at an average elevation of approximately 5 km above sea level, is 5 to 8 km thick and extends east-west for roughly 550 km (Orme et al., 2014). The Xigaze strata record facies transitions from deep to shallow to marginal marine, and finally to non-marine fluvial facies. Xigaze stratigraphy is divided into two groups: Lower to Upper Cretaceous Xigaze Group and the Upper Cretaceous to Lower Eocene Tso Jiangding Group (Region, 1993), the latter of which is the focus of this study. An absence of forearc strata <51 Ma suggests sedimentation in the forearc basin ceased at this time, or has been subsequently eroded, possibly due to uplift of the suture zone related to continental collision.

2.2. Tso Jianding Group

The Tso Jiangding Group (S. Tibet) records a general shoaling upward trend coincident with the closing Tethys (Orme et al., 2014). This group can be divided into four formations whose facies associations trace the change from deep to shallow marine environments: the Padana, Qubeiya, Quxia, and Jialazi Formations. The latter three formations are only preserved in the vicinity of the sampling locality at the westernmost end of the Xigaze forearc basin northwest of Saga (see Fig. 1c). The abundantly fossiliferous marine limestones analyzed in this study belong to the youngest unit, the Jialazi Formation. This unit

consists of 145-400 meters of fossiliferous limestone, packstone, and floatstone interbedded with 25-50 meter thick siltstone, sandstone and conglomerate sequences and thin lenses of pale gray shale. The age of the Jialazi is constrained as 62 to 51 Ma by biostratigraphy (Eocene *Nummulites*), Ypresian-age zircons in sandstones near the top of the section, and a 53.8±0.7 Ma tuff in the lower part of the formation (Orme et al., 2014; Ding et al., 2005; Hu et al., 2015; Aitchison et al., 2011; Wan et al., 1998).

2.3. Thermal history of the Jialazi Fm

Zircon and apatite grains were collected from the Jialazi Formation of the Tso Jianding Group by Devon Orme for (U-Th)/He thermal modeling. (U-Th)/He data are reported in Orme (2017). Modeled thermal histories of the Tso Jianding Group are characterized by burial to temperatures >180 to <200°C (∼7 to 8km depth) at by ∼21 Ma, followed by fairly linear and rapid cooling/exhumation associated with the Gangdese and Great Counter Thrusts (Orme, 2017). The ZHe ages from the 53.8±0.7 Ma tuff in the lower Jialazi Fm are reset and range from 20 to 30 Ma (Orme, 2017). Cooling appears to be monotonic below 60°C between 8 and 5 Ma (Orme, 2017).

3. Methods

3.1. Sample collection

Five shales, thirty carbonates, and three ash beds were collected from Jialazi Formation sections described in (Orme et al., 2014) and adjacent sections (Fig. 1). For consistency, section labels in this study are those used in Orme et al. (Orme et al., 2014). The lower Cenozoic Section E samples are dominantly fossiliferous, shallow marine limestones with variable quartz sand content. Stable and clumped isotope samples range from carbonate micrite to sandy limestone, packstone, and floatstone. Late Paleocene to early Eocene Sections F-H record the transition from shallow marine to non-marine coastal plain deposition. The marine lime mudstones collected from Section F contain abundant foraminifera

Nummulites Discocyclina. Sparse paleosols were sampled from the upper 72 m of Section F. The red-green paleosol beds are interpreted as periods of low to no flow in overbank channel deposits formed during progradation of the coastal plain fluvial system (Orme et al., 2014). The conformable transition from marine to fluvial deposition in the Jialazi Formation correlates to high-flux magmatism of the Gangdese arc in the Eocene (Chung et al., 2005; Lee et al., 2009). The remainder of the samples collected in sections G and H are paleosol carbonate, shales, and ashes.

3.2. Micro-sampling

Samples were powdered using a Foredom TX low speed drill with a Brasseler US#2 HP Round bit at low speed to avoid significant frictional heating. Powders sampled by the Foredom drill typically resulted in powder extraction over a 15 to 20 mm^2 area. This practice effectively mixes any isotopic heterogeneity over the drilled area, but careful attention was paid to only drill within same-texture domains. Additional sub-samples (fossil shells, foraminifera, veins, and micrite within individual 2.5×4×0.5 cm thick sections; Fig. 2c) were powdered using a New Wave Research micromill with a 300m tungsten carbide bit (Brasseler #H52.11.003) for higher spatial resolution carbon, oxygen, and clumped isotope analyses to differentiate alteration behavior of carbonate material type. Due to the relatively large sample mass required for clumped isotope measurements on the MAT253 and to make sure only one texture or fossil was sampled, in some cases, only enough sample powder was extracted for one clumped isotope analysis.

3.3. Stable isotope and clumped-isotope measurements

Carbonate $\delta^{18}O$ and $\delta^{13}C$ were measured at the University of Chicago on the Thermo-Finnigan 253 isotope-ratio mass spectrometer (IRMS) and Delta V IRMS coupled to a GasbenchII. MAT253 $\delta^{18}O_{CO_2}$ measurements are converted to $\delta^{18}O_c$ compositions using a calcite-CO_2 fractionation factor ($\alpha_{CO_2-CO_3}$) associated with phosphoric acid digestion (Wachter and Hayes, 1985; Swart et al.,

1991; Guo et al., 2009) at 25°C. Stable and clumped isotope sample preparation, analyses, and data treatment are outlined in the Supplemental Information.

The Zaarur et al. (2013) Δ_{47}-temperature calibration was applied to the clumped isotope data to calculate Δ_{47}-derived temperature estimates. More recently, a number of Δ_{47}-temperature calibrations have been published with higher reported precision due to a greater number of samples and wider temperature distribution. However, the carbonate digestions used to construct these more robust calibrations were at 75 to 90°C. Carbonate digestions and CO_2 purification are performed on a glass vacuum extraction line at 25°C at The University of Chicago, most similar to the protocol followed during the preparation of the Zaarur et al. (2013) Δ_{47} thermometer; for this reason, the Zaarur et al. (2013) thermometer was chosen because of unresolved differences in Δ_{47}-T slope at different acid digestion temperatures. Δ_{47} errors were determined at the 95% confidence level using the ordinary least squares regression in Zaarur et al. (2013) (Fig. S1.

3.4. Optical and cold-cathode cathodoluminescence microscopy (CL)

Thirty μm-thick geological thin sections were optically screened for potential alteration fabrics using plane light and cathodoluminescence (CL) petrography, and compared to coeval large benthic foraminifera from the Ocala Fm. The Ocala Fm formed on the Florida bank in the Eocene and has never been buried more than 300 m (D. Budd, communication). Therefore, the Ocala Fm provided relatively pristine specimens with which to compare preservation of primary morphologies, microstructures and growth fabrics of the large benthic foraminifera abundant in the Jialazi Fm.

Relative timing, or "generations", of primary and post-depositional carbonate crystallization are recorded by variations in luminescence (Snell et al., 2013, 2014; Huntington et al., 2011; VanDeVelde et al., 2013). Luminescence intensity reflects the relative abundances of the reduced forms of elemental iron, Fe^{2+} (dominant quencher of carbonate luminescence), and manganese, Mn^{2+} (dominant activator; Budd et al. (2002); Marshall (1988)). Variation in CL is

thought to reflect the redox conditions of the depositional and post-depositional environments in which calcite forms (Barnaby and Rimstidt, 1989). Oxidizing environments (e.g. shallow marine) produce dull or non-luminescence because Fe^{2+} and Mn^{2+} are not readily available. However, carbonate formed during deeper burial will produce brighter luminescence (Solomon and Walkden, 1985; Boggs and Krinsley, 2006). Luminescence zonation is indicative of chemical heterogeneity in calcite formation conditions (Sommer, 1972; Solomon and Walkden, 1985; Budd et al., 2002), and thus multiple calcite generations. Variations in luminescence distribution are mapped in micrite, foraminifera, bivalve and gastropod shells, and calcite cements in shell body cavities to identify evidence of secondary carbonate precipitation in different diagenetic settings. The cold-cathode luminoscope at Miami University is mounted directly onto the stage of a petrographic microscope. The benefit of using a cold-cathode cathodoluminoscope, rather than microprobe, is the capability to directly compare optical and CL petrography of the exact same site in real-time (Fig. 5). The images were taken at a vacuum of ∼90 mTorr with a beam strength of 0.80 to 0.83 mV.

4. Results

4.1. Isotopic results

The Jialazi Fm shallow marine carbonates are ^{18}O-depleted (–12 to –21 ‰ VPDB; Figure 2; Table S1) relative to low latitude Paleogene marine mollusks (Kobashi et al., 2001), benthic foraminifera (Miller et al., 1987), and fish otoliths (Ivany et al., 2003). Carbon isotopic compositions of the marine samples range from –3.6 to 0.8 ‰ VPDB. The groundwater and paleosol carbonates from the near-shore fluvial-deltaic system conformably above the shallow marine section yield $\delta^{18}O_c$ values of –15.4 to –29.5 ‰ , with one paleosol yielding a value of –0.4 ‰ . Carbon isotopic compositions of the terrestrial carbonates ranged from –4.0 to –9.7 ‰ VPDB.

Δ_{47} measurements from the shallow marine Jialazi Formation samples range from 0.460 to 0.721 relative to the carbon dioxide equilibrium scale and 25°C

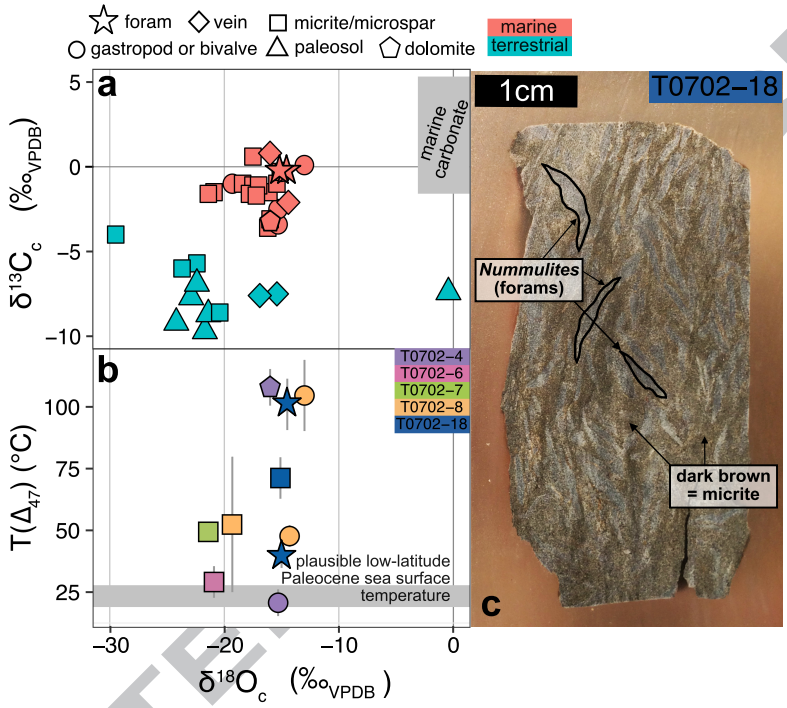

Figure 2: δ^{13}**C,** δ^{18}**O, and** Δ_{47} **values of Paleocene-Eocene Jialazi Fm marine (light red) and fluvial-lacustrine (blue-green) carbonates. A.** Late Paleocene-Early Eocene low-latitude, shallow marine carbonate compositions (gray box) are plotted for reference, and are derived from mollusks (Kobashi et al., 2001), benthic forams (Miller et al., 1987), and fish otoliths (Ivany et al., 2003). **B.** Marine Jialazi Fm clumped isotope temperatures (T(Δ_{47})) plotted relative to $\delta^{18}O_c$, and plotted by carbonate type (shape) and individual samples (color). (c) T0702-18 billet as an example of proximity of sub-sampled carbonate components in individual samples.

acid digestion temperature ($\Delta_{47,\mathrm{CDES25}}$; Dennis et al. (2011); Fig. 2), or ~20 to 110°C using the Zaarur et al. (2013) Δ_{47} thermometer for low temperature carbonate digestion. The oxygen isotope calcite-water fractionation factor (Kim and O'Neil, 1997) is calculated using the measured T(Δ_{47}), and $\delta^{18}O_w$ is calculated assuming equilibrium carbonate precipitation at T(Δ_{47}) (Table S2; Fig. 7).

4.2. Field, hand sample, and petrographic observations

Micro-scale fractures were rarely observed in thin section. Stylolites were identified along the boundaries between foraminifera tests and micrite and silt matrix in some of the fossiliferous floatstones (Fig. 4e). Primary shell morphologies and internal fabrics are preserved in many of the biogenic carbonate types (i.e. gastropods, foraminifera, and bivalves). Shell void spaces are filled primarily with silt-size quartz in a microspar carbonate matrix. Fossils within the marine limestones and siltstones appear to have undergone variable amounts of alteration and mineral replacement. Occasional biogenic carbonate has undergone extensive replacement of primary calcite to sparry calcite with large, well developed crystal domains (e.g. gastropod in Fig. 3e and f). However, another gastropod shell from the same sample retains primary cross-lamellar microstructure (Fig. 3c, d). Two other shells of comparable size on this slide display evidence of minor sparry calcite replacement, and maintain primary growth features (i.e. growth bands). Differential alteration of primary microstructures within individual samples is characteristic of all samples from this stratigraphic section.

The test edges of foraminifera from both the Ocala and Jialazi Fms display some degree of dissolution due to the natural perforated texture of *Nummulites* tests (Fig. 4c-e). The chambers of Jialazi Fm forams are spar filled, whereas the chambers of the Ocala Fm forams remained empty during burial. The fibrous internal growth fabric of the test walls is well-preserved in both the Ocala and Jialazi Fms (Fig. 4e-g), with little to no bulk recrystallization of primary test material.

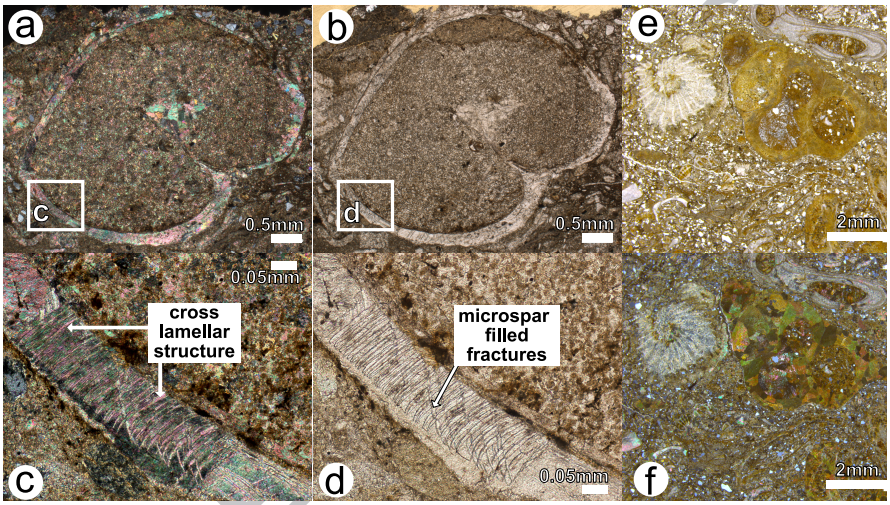

Figure 3: **Petrographic screening of fossiliferous limestones, packstones, and floatstones of the Tso Jiangding Group.** Shell and foraminifera test morphologies are retained throughout the burial history of these samples, as seen in plane polar light (**B, E**). The internal morphology of fossils are variably preserved, as seen in cross polar light (**C** [cross-lamellar structure], **F** [spar domains in gastropod; growth bands]).

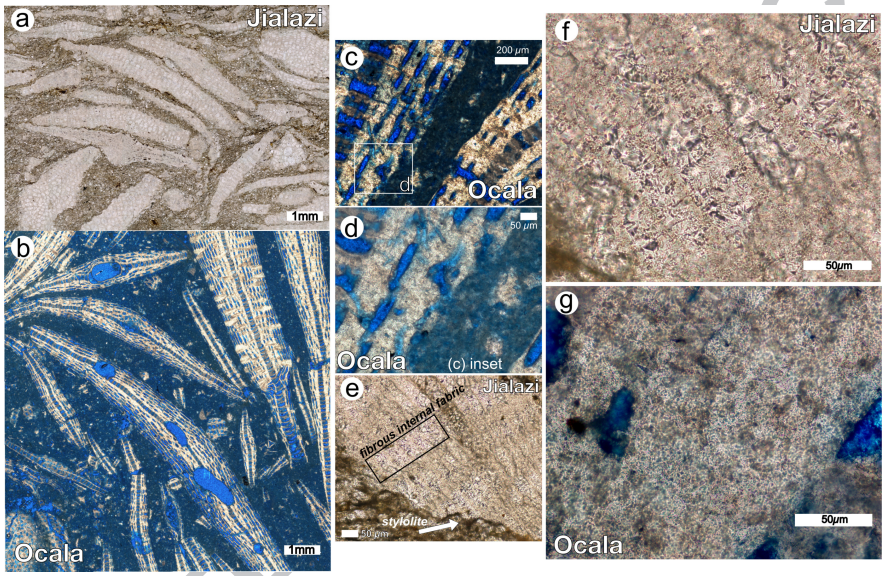

Figure 4: **Comparative petrography of Paleocene-Eocene large benthic foraminifera. A., E., F.** Paleocene-Eocene Jialazi Fm *Nummulites Discocyclina*. **B., C., D., G.** Eocene Ocala Fm *Nummulites Discocyclina* and *Lepidocyclina*. **C., D.** Ocala Fm foram tests display some amount of dissolution in fuzzy test edges. **E.** Pressure dissolution is the most prevalent example of minor dissolution in Jialazi Fm foraminifera. **F., G.** Jialazi and Ocala Fms preserve similar degree of fibrous internal fabric.

4.3. Cathodoluminescence

Observations and interpretations of CL petrography focuses primarily on a foraminifera-rich floatstone, T0702-18 (Fig. 5). Sample T0702-18 varies from non-luminescent to bright red-orange. The cement binding the silt between foraminifera in T0702-18 (see Fig.5g) is dull to non-luminescent. The non-luminescent areas in CL (Fig. 5b, d) correspond to 20 to 30 μm-diameter crystals, indicative of neomorphic overgrowth. Overgrowths can form by re-structuring the original biogenic calcite, thus preserving the original low-Mn composition indicated by the suppressed luminescence.

Fig. 5a-b display the structural preservation of the septa and chamber framework of a *Nummulites Discocyclina*. The septa has brighter luminescence than the marine cement surrounding the lenticular fossils. The shell-filling microspar displays the brightest luminescence. Dissolution surfaces are seen much more clearly in CL than PPL (Solomon and Walkden, 1985). Preserved dull luminescence in the interior of foraminifera tests and brighter luminescence along the exterior is common (Fig. 5f). The edges of the foraminifera in Fig. 5f display bright red-orange luminescence. Secondary dissolution-precipitation occurs at the boundary between the foraminifera and matrix in Fig. 5e, f.

5. Isotopic modeling and discussion

Low-latitude, shallow marine seawater was likely 20 to 30°C with an oxygen isotopic composition of ∼0 to –1‰ VSMOW (Kobashi et al., 2001). Today, the Jialazi Fm carbonates record $\delta^{18}O_c$ values of –12 to –21‰ VPDB, which are substantially more ^{18}O-depleted relative to their inferred original marine $\delta^{18}O_c$ composition (∼-2‰ VPDB (Kobashi et al., 2001); Fig. 2), and therefore require significant water-rock alteration. Importantly, sub-samples yield low T(Δ_{47}) similar to shallow marine temperatures and retain primary carbonate fabrics after extensive secondary mineralization with ^{18}O-depleted fluid (Fig. 6). Here, water-rock isotope exchange reactions and solid-state reordering models are explored with a goal of determining the most likely burial alteration histories

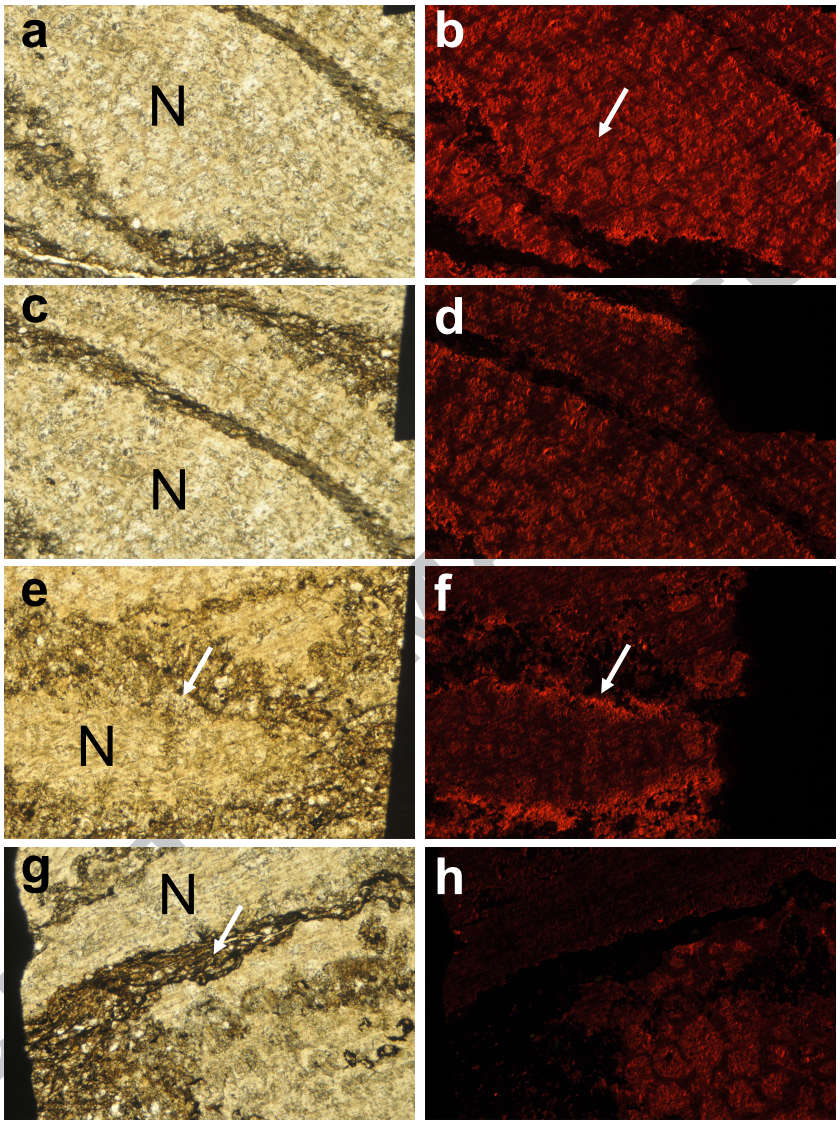

Figure 5: **Paired plane polar light (PPL; A., C., E., G.) and cathodoluminescent (CL; B., D., F., H.) petrographic images of sample T0702-18.** *Nummulites Discocyclina* foraminifera are labeled with an "N". White arrows point to areas described in the text. The width of each image is 2 mm.

that can yield $\delta^{18}O_c$ values >10‰ lower than original compositions, and yet, retain many primary carbonate fabrics and biogenic morphologies, and yield low $T(\Delta_{47})$ values. The $\delta^{18}O_c$ values of open- and closed-system water-rock reaction alteration products are calculated at varying temperatures (∼burial depths) and W:R, and within thermokinematic constraints, following the equations of Banner and Hanson (1990). Finally, the empirically derived reordering models of Stolper and Eiler (2015) and Passey and Henkes (2012) are used to estimate the effects of solid-state reordering.

5.1. Water-rock isotopic exchange modeling

To develop an alteration history of the Jialazi Fm carbonates, the equilibrium isotopic exchange reactions of Banner and Hanson (1990) are employed to calculate equilibrium values of $\delta^{18}O_w$, $\delta^{18}O_c$, and $T(\Delta_{47})$ (Fig. 7) within three probable scenarios under which the Jialazi Fm carbonates were altered by diagenetic fluids: (1) a Paleocene shallow marine or shallow burial environment, (2) deep burial diagenesis, and (3) late-stage recrystallization on the retrograde path or at the Earth's surface post-exhumation.

For carbonate rocks that have undergone high-temperature diagenesis, carbonate Δ_{47} should be considered an integrated product of multiple recrystallization events and variable degrees of solid-state reordering during deep burial rather than the temperature of equilibrium carbonate precipitation during one recrystallization event. However, using $T(\Delta_{47})$ as an equilibrium temperature simplifies assumptions used in water-rock reaction modeling and tests whether the homogeneous $\delta^{18}O_c$ values paired with Δ_{47} variability records sequential alteration events at discrete temperatures ($T(\Delta_{47})$), from which $\delta^{18}O_w$ of the diagenetic fluids may be calculated. One alternative hypothesis is that the majority of water-rock alteration occurred under high-temperature burial conditions, but the $T(\Delta_{47})$ of burial was subsequently and differentially overprinted during lower temperature alteration on the retrograde path.

The calculated $\delta^{18}O_c$ values from each alteration scenario (T, initial $\delta^{18}O_c$, diagenetic $\delta^{18}O_w$, and W:R) are compared to the measured $\delta^{18}O_c$ values to

assess the relative contribution of each diagenetic step to the final product. An average marine carbonate $\delta^{18}O_c$ value of –2‰ is used as the initial isotopic composition in time step 1 (t_1). A $\delta^{18}O_w$ value of –4‰ VSMOW is used for low-elevation meteoric water (Quade et al., 2011). This value is extrapolated from modern low-elevation stream waters from the Siang Tsangpo Basin (259 to 612 m above sea level [m.a.s.l.]) southeast of the Himalayas (Hren et al., 2009), which range ∼–7 to –5‰ VSMOW, assuming that meteoric water both at sea level and formed in the Eocene would have slightly higher $\delta^{18}O$ values. Modern $\delta^{18}O_w$ values of high elevation meteoric water on the Tibetan Plateau (Garzione et al., 2000; Bershaw et al., 2012) were used in water-rock exchange reactions during later stage recrystallization (T=10 to 30°C) to yield lower $\delta^{18}O_c$ values and low T(Δ_{47}) (scenario 3). The equilibrium alteration product of the initial carbonate is calculated under a range of W:R conditions (0 [rock-buffered] to 14 [water-buffered]), with fluids of plausible compositions and temperatures (Fig. 6).

The settings in which the Jialazi Fm samples could have recrystallized can be inferred based on the water-rock exchange calculations and measured values. In a rock-buffered system, even under high temperature conditions, $\delta^{18}O_c$ is relatively buffered from water-rock exchange and, thus, can retain an unaltered composition close to that of the primary $\delta^{18}O_c$ (see low W:R alteration products in Fig. 6 and gray arrows in Fig. 7a,b). However, even minimal exchange occurring over a geologically relevant interval under rock-buffered conditions (low W:R) can have a cumulative W:R (total fluid flow through a finite volume rock package since deposition) approximating higher W:R conditions in an open-system (Banner and Hanson, 1990). Under higher W:R conditions, the carbonate composition is driven towards that of the fluid (Fig. 6; yellow and blue arrows in Fig. 7a,b), with the relationship between the two governed by the temperature-dependent water-carbonate oxygen isotope fractionation: $\alpha(T)=(\delta^{18}O_c+1000)/(\delta^{18}O_w+1000)$, with $1000*\ln(\alpha(T)) = 18030/T - 32.42$ for calcite (Kim and O'Neil, 1997). In general, water-rock exchange proceeds faster at higher temperatures and, in turn, $\delta^{18}O_c$ and $\delta^{18}O_w$ values approach equilib-

rium. The following sections discuss the likelihood of alteration in each of the three aforementioned settings (i.e. temperature and $\delta^{18}O_w$) within the context of water-rock isotope exchange modeling, petrography, and solid-state reordering.

5.2. Phases 1a and b: Early marine and shallow burial diagenesis

Numerous recent studies have demonstrated the importance of early marine diagenesis and diagenesis in the upper 0.5 to 1 km of the subsurface for the isotope and trace element geochemistry of the sediments (Fantle and Higgins, 2014; Fantle, 2015; Higgins et al., 2018; Ahm et al., 2018; Stolper et al., 2018). The preservation of primary external shell morphology within the marine limestones and floatstones of the Jialazi Fm (Fig. 3) suggests that pore- and void-filling microspar cementation is either syngenetic with the carbonaceous marine mud (Munnecke et al., 1997) or a product of early, shallow burial diagenesis (Choquette and Pray, 1970). This early cementation and void-filling allowed shells to maintain their structural integrity during burial compaction, which reduces porosity and permeability by both physical and chemical processes (Choquette and Pray, 1970) (Fig. 4a). It is also possible that the early microspar cementation, in some cases, protected primary carbonate material from later replacement. For example, in Fig. 3, a gastropod shell is encased in muddy sediment likely derived from a compositionally similar marine setting, and therefore there is not a strong geochemical gradient between the shell and adjacent infill and the shell carbonate remained relatively stable. The preservation of cross-lamellar microstructure and outer prismatic layer visible in cross polar light demonstrates this enhanced preservation. Finally, the elongate and radial fabrics of the spar found within the gastropod shells and foram tests are indicative of fast precipitation due to the high saturation state of calcite in shallow marine water.

Although a significant amount of carbonate precipitated during early diagenesis, the oxygen isotopic composition of the diagenetic fluids would have been relatively similar to seawater and have at most a minimal effect on car-

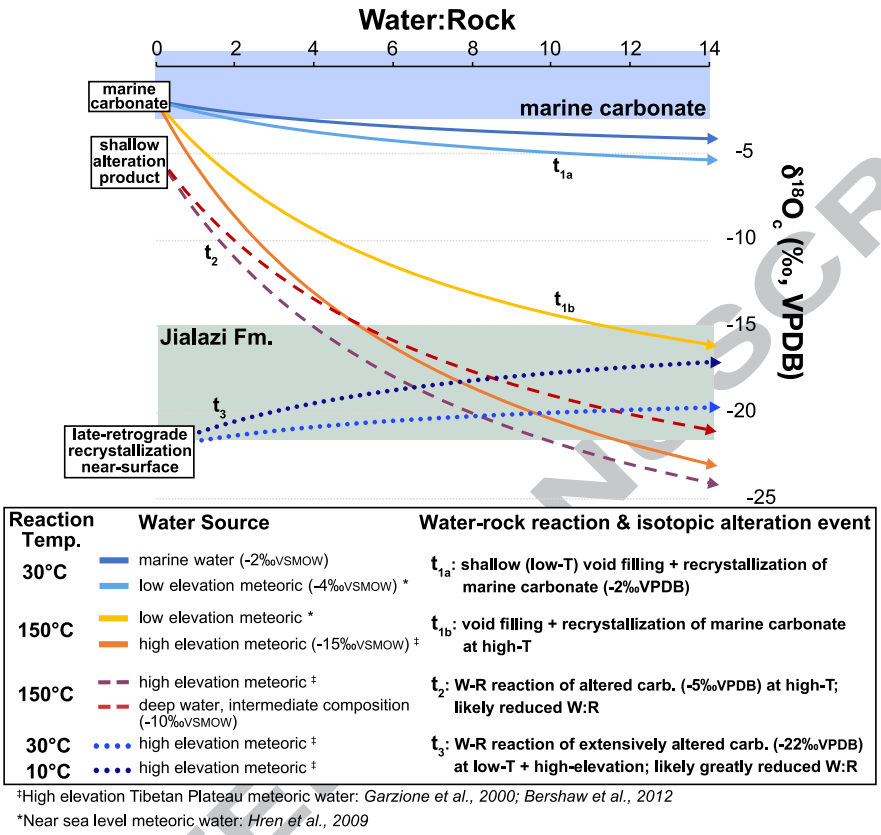

Figure 6: **Potential water-rock alteration scenarios (W:R, $\delta^{18}O_{water}$, $\delta^{18}O_c$) and their equilibrium carbonate products using the isotopic exchange reactions of Banner & Hanson (1990).** Oxygen isotopic compositions of early Cenozoic marine carbonate and Jialazi Fm carbonates are marked by blue and green boxes, respectively. t_{1a} and t_{1b} represent isotopic alteration of the original marine carbonate during early marine diagenesis and deep burial temperatures, respectively. t_2 displays possible alteration products of deep burial starting with early marine diagenesis alteration products. t_3 represents the minimal amount of oxygen exchange that can occur post-exhumation at low temperatures with high elevation meteoric water. The text box provides the reaction temperature (representing alteration during shallow or deep burial), $\delta^{18}O$ of the altering fluid (approximately marine, low-elevation precipitation from south of the Himalaya (Hren et al., 2009), and modern Tibetan meteoric water (Garzione et al., 2000; Bershaw et al., 2012)), and water-rock exchange scenarios as described in text.

bonate $\delta^{18}O$ (t_{1a} in Fig. 6). Because Δ_{47} of altered carbonate is thought to record a mixture of the Δ_{47} of primary and diagenetic constituents, changes in Δ_{47} are insignificant at burial depths <1 km (Stolper et al., 2018). Below ~1km, the cumulative W:R is large enough for the Δ_{47} value of the secondary carbonate constituent to affect the bulk Δ_{47} value. Overall, early marine diagenesis almost certainly occurred within the Tso Jianding sediments, evidenced by spar infill within biogenic voids and minor dissolution rims on the test edges of foraminifera, but the secondary carbonate precipitated during these eogenetic events probably did not have a significant impact on the stable isotopic compositions of the original carbonate.

5.3. Phase 2: Water-rock exchange during deep burial

As described above, carbonate minerals from the Jialazi Fm have been buried to at least 180°C and, thus, likely recrystallized at a range of temperatures and fluid compositions. Alteration of the bulk oxygen isotopic composition of these marine carbonates requires pathways by which water may be introduced to compacted limestones with negligible porosity that should leave micro-scale geochemical and/or textural fingerprints. During tectonic unroofing, cm- to meter-sized decompression-related fractures can provide pathways for groundwater to interact with the exhuming strata. While no large fissures were identified in the field, small, sparry calcite-filled fractures along shell-matrix boundaries (Fig. 3) demonstrate that some amount of diagenetic fluid was able to penetrate the compacted rocks and provide opportunity for isotopic exchange. Dissolution textures are more prevalent along the foraminifera edges while the interior of the tests remains relatively unaltered. This may be caused by the geochemical gradient imposed by proximity to infiltrating diagenetic fluids during burial. Dissolution rims around foraminifera and shells (Fig. 4) could be pressure solution seam, similar to stylolites, formed with water with a higher concentration of a calcite luminescence activator, Mn^{2+} (Marshall, 1988), than the primary marine water. Regions of bright luminescence related to pressure solution, although not pervasive, could point to physical evidence of the wholesale oxygen

exchange mechanism that drove the pervasive $\delta^{18}O_c$ alteration.

$\delta^{18}O_c$ is mostly homogeneous across individual samples, with some examples of a ~5‰ difference between carbonate components (fossils, micrite/microspar). Based on $\delta^{18}O_c$ alone, the Jialazi Fm samples are interpreted as products of extensive recrystallization during burial and exhumation. However, large within-sample T(Δ_{47}) heterogeneity precludes this simple explanation. For example, three separately drilled micrite powders from sample T0702-8 yield T(Δ_{47}) values of ~28°C, ~56°C and ~72°C, but all yield a $\delta^{18}O_c$ of ~–19.5‰ . The individual T(Δ_{47}) values could possibly record temperatures of discrete intervals of alteration with waters of $\delta^{18}O_w$ compositions ranging ~–9 to –17‰ VSMOW, or the entire sample recrystallized with the same ^{18}O-depleted waters during burial to yield a $\delta^{18}O_c$ close to the measured value (–19.5‰ VPDB). In Fig. 6, t_2 displays possible alteration products of deep burial starting with carbonate previously altered during early marine diagenesis. Because all high-T water-rock exchange reactions can yield the measured $\delta^{18}O_c$ values at W:R>3 to 4 and $\delta^{18}O_w$ <–4‰ VSMOW, we cannot distinguish between the aforementioned alteration pathways with water-rock modeling alone. However, the Jialazi Fm samples experienced temperatures at or above the ZHe closure temperature (~160°C) long enough for diffusive loss of ZHe (Dodson, 1973), and thus, all carbonate in this stratigraphic package theoretically should have undergone at least partial reordering of carbon-oxygen bonds to a more stochastic distribution of ^{13}C-^{18}O clumps (i.e. lower Δ_{47}, higher apparent T(Δ_{47})). Therefore, the low T(Δ_{47}) measurements must have formed by recrystallization after deep burial solid-state reordering, supporting the second hypothesis of bulk alteration during deep burial.

Finally, micrite and cements yield lower $\delta^{18}O_c$ values (i.e. further from primary marine composition), and thus, are interpreted to have undergone more extensive recrystallization in the presence of ^{18}O-depleted fluids (Fig. 7a). The duller luminescence of shell materials compared with their void-filling microspar (Fig. 5) provides further evidence of material-specific resistance to alteration. The brighter luminescence of the void-fill microspar could reflect a greater degree

of recrystallization, and thus oxygen exchange, with water with a greater supply of Mn^{2+} and Fe^{2+} cations in a deeper burial setting (Marshall, 1988; Huntington et al., 2011). Therefore, under less extreme burial conditions, biogenic carbonate may more faithfully retain primary environmental information than micrite and other carbonate materials. Regardless, at $T(\Delta_{47})>75°C$, there is less of a $\delta^{18}O_c$ difference between material types, providing additional evidence for bulk recrystallization during high-temperature deep burial conditions.

5.4. Phase 2b: Solid-state internal isotopic exchange

Both the Stolper and Eiler (2015) and Passey and Henkes (2012) solid-state reordering models are employed to explore how Δ_{47} of a shallow marine carbonate evolves through a given time-temperature burial history (Fig. 8). The initial conditions of the first model run is a $\Delta_{47CDES25}$ equal to a shallow marine depositional temperature of 25°C. Separate empirically derived kinetic parameters are used for calcite (Passey and Henkes, 2012; Stolper and Eiler, 2015) and dolomite (Lloyd et al., 2018). The best-fit time-temperature history from Orme (2017) is used to derive the ambient temperature at each time step based on thermokinematic modeling from ZHe and AHe ages of tuff-derived zircons from the Jialazi Fm near Saga, southern Tibet.

Because extensive recrystallization occurred on the prograde burial path, the initial carbonates in a second set of experiments begin with a Δ_{47} value lower than the original marine value, representing new carbonate material recrystallized at an elevated burial temperature and then reordered in the solid-state (Fig. 9). In these model runs, I use the Schauble et al. (2006) $T(\Delta_{47})$ calibration to calculate Δ_{47} from the ambient temperature on the Orme (2017) t-T path as the initial Δ_{47}, and run the forward model from that time point to 0 Ma along the same t-T history.

Δ_{47} is expected to "collapse" to one value or a narrow range of values during reordering, irrespective of the starting Δ_{47}, rather than creating Δ_{47} dispersion among data from one thermal history (Cummins et al., 2014). The modeling experiment confirms this expectation for calcite (Fig. 9a), but not dolomite (Fig.

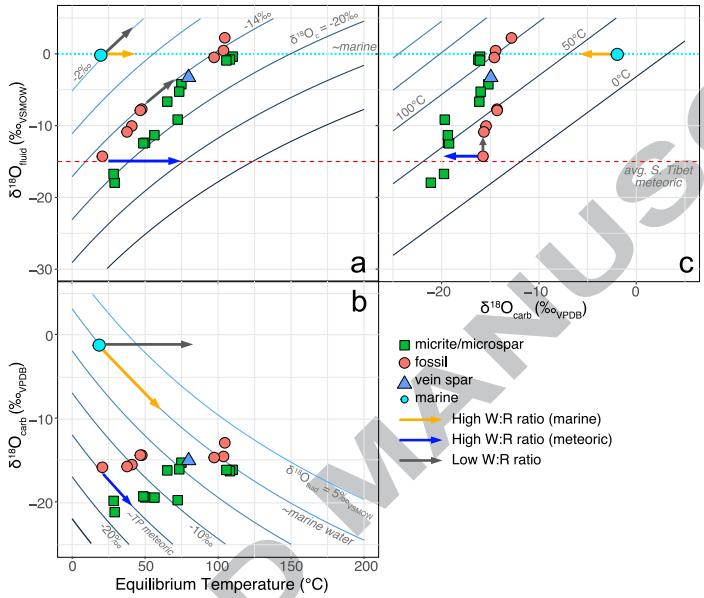

Figure 7: **Equilibrium calculations of $\delta^{18}O_w$ using $\delta^{18}O_c$ and T(Δ_{47}). A.** $\delta^{18}O_w$ of marine and average high elevation Tibetan Plateau meteoric water (Garzione et al., 2000; Bershaw et al., 2012) are marked with dotted and dashed lines. Contours represent isotherms (**B**) and isotope contours of carbonate (**A**) and water (**C**) $\delta^{18}O$. Colored arrows mark the direction in which carbonate composition would alter under varying water-rock ratios (gray: low W:R) and fluid composition (yellow: marine; blue: meteoric). As seen in **A**, micrite/microspar $\delta^{18}O_c$ compositions are divided above and below ~75°C, which may indicate two alteration events. Biogenic carbonates have consistent $\delta^{18}O_c$ values of ~–14 ‰ VPDB, which would require a range of $\delta^{18}O_w$ values from marine composition to –15‰ VSMOW. This likely indicates that Δ_{47} records later alteration, and not conditions under which the bulk $\delta^{18}O_c$ alteration occurred.

9b). Regardless of the starting Δ_{47}, reordered calcite Δ_{47} falls between the Δ_{47} of reordered marine carbonate (∼0.540) and Δ_{47} of the maximum burial temperature (∼0.450). Dolomite has a higher threshold temperature for reordering and slower reordering kinetics (Lloyd et al., 2018). Within the range of Jialazi Fm burial temperatures (<180°C), very minimal reordering occurs within the dolomite crystal lattice, and therefore, the single dolomite measured from this section (T0702-4) likely records the temperature of dolomitization, or the time at which Mg-enriched fluids infiltrated the buried Jialazi sequence, rather than solid-state reordering. Mg-rich fluids could have been derived from magnesium silicates from the Gangdese batholith and coeval Linzizong volcanics at these burial depths (Schärer et al., 1984; Yin and Harrison, 2000; He et al., 2007; Wen et al., 2008). The majority of the Jialazi carbonates were not dolomitized, and therefore, dolomitization either occurred under very low W:R conditions or the Mg-rich fluid became depleted before further dolomitization could occur.

Results of the paired modeling exercises demonstrate that all $\delta^{18}O_c$ measurements and T(Δ_{47}) measurements >75°C can be explained by prograde recrystallization followed by solid-state reordering. However, T(Δ_{47}) <75°C, and the inter- and intra-sample Δ_{47} variation, requires an alteration mechanism at near-surface conditions.

5.5. Phase 3: Low-temperature alteration during exhumation

Only a minimal amount of $\delta^{18}O_c$ alteration is expected to occur at low temperature with high elevation meteoric water under low W:R conditions (t_3 in Fig. 6), supporting the interpretation that the pervasive oxygen isotope exchange occurred at depth. However, it is inferred that enough water-rock recrystallization occurred on the retrograde path to yield differential Δ_{47} values. Although alteration reactions on the retrograde path were likely rock-buffered due to burial compaction, small differences in available pore space could have allowed very minimal and variable recrystallization. Small differences in W:R ratio under low W:R conditions has a greater effect on the resultant $\delta^{18}O_c$ of the altered carbonate than the same magnitude of W:R change under high W:R

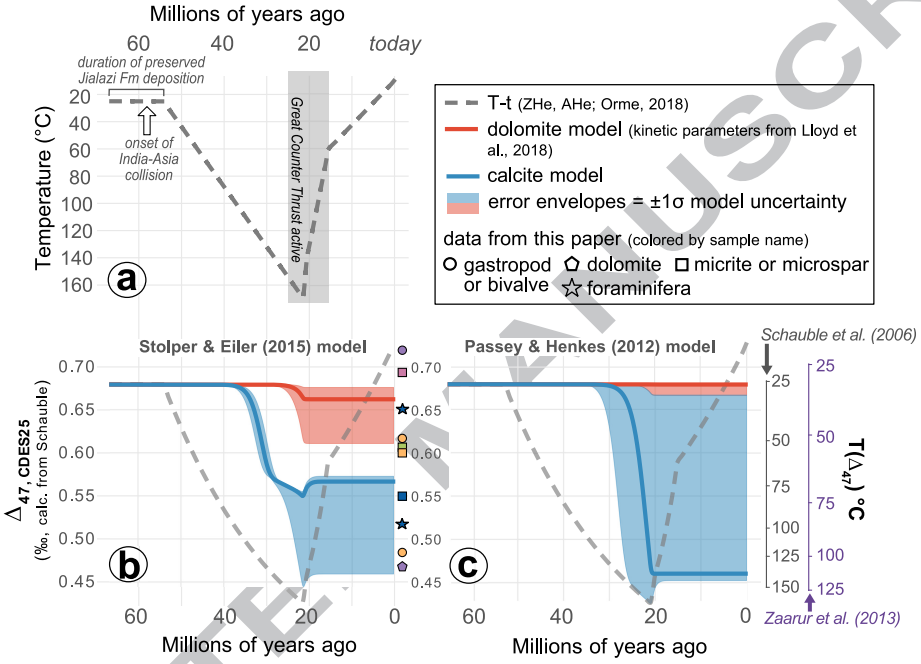

Figure 8: Δ_{47} **resetting due to solid-state reordering during burial and unroofing.** (a) Simplified time-temperature path for the Jialazi Formation from Orme (2017) with key tectonic events related to this sedimentary basin labeled. (b) and (c) Time-Δ_{47} evolution by solid-state reordering through two models ((b) Stolper and Eiler (2015) and (c) Passey and Henkes (2012)) starting with a plausible Paleocene low-latitude sea surface temperature of 25°C and the Schauble et al. (2006) Δ_{47} thermometer.

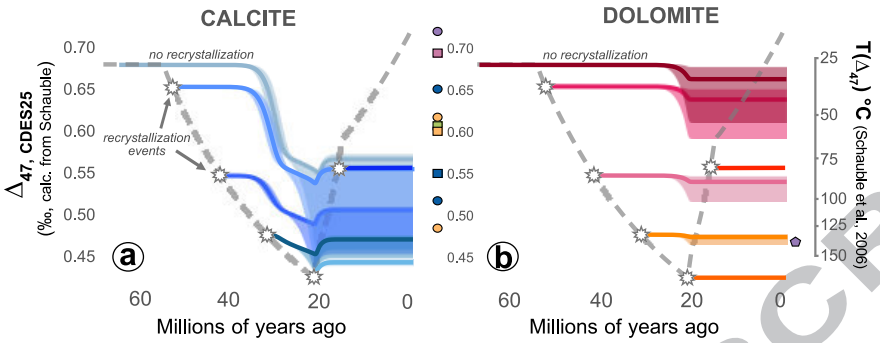

Figure 9: **Reordering recrystallized (a) calcite and (b) dolomite.** Gray and white stars mark recrystallizaiton events on the prograde and retrograde. The recrystallized mineral records a new Δ_{47} value equal to the ambient temperature of recrystallization, overprinting the original mineral formation temperature. The Stolper and Eiler (2015) reordering model was run starting from new initial Δ_{47} values reflecting recrystallization along the time-temperature path in 5-10 My increments.

conditions (Fig. 6). It is possible that, similarly, the breaking and creation of new C–O bonds under variable, low W:R could have a more significant impact on Δ_{47} values than the same magnitude of W:R variability at higher W:R. If so, recrystallization under variably low W:R would yield a heterogeneous distribution of ^{13}C-^{18}O bonds within an individual sample. This could explain Δ_{47} variability such as the micrite and two *Nummulites* from sample T0702-18 (Fig. 2), which yield T(Δ_{47}) of $\sim 79^{+9}_{-7}$°C, 39±4°C and 101^{+11}_{-9}°C, respectively. These T(Δ_{47}) values likely do not record the precise temperatures at which the individual carbonate sub-samples recrystallized, but instead record relative mixtures of new carbonate material formed in the near-surface and higher temperature diagenetic settings. Finally, using the traditional isotope exchange reactions of Banner and Hanson (1990), late-stage recrystallization with meteoric water at a temperature as cold as ~25°C would require an exceptionally high water:rock ratio. Thus, a mechanism is still required to explain the impetus for carbonate alteration at near-surface temperatures, as well as the preservation of primary textures and structures during the magnitude of isotopic alteration within the

Jialazi Fm.

Stable mineral recrystallization, a mechanism of atomic exchange between mineral and dissolved reservoir at relatively cool temperatures (<100°C) in which carbonate components retain their original fabrics, morphologies, and microstructures (Gorski and Fantle, 2017), could have driven variable yet wholly pervasive isotopic alteration within the Jialazi Fm in the near-surface without overt changes to the mineralogy or structures. Recent experiments have demonstrated that elemental and isotopic exchange can proceed to near-equilibrium on experimental timescales even at temperatures below 100°C (Stipp et al., 1992; Handler et al., 2009; Frierdich and Catalano, 2012; Curti et al., 2010; Avrahamov et al., 2013; Lestini et al., 2013; Handler et al., 2014), or as cool as a shallow marine diagenetic setting (Fantle, 2015). The magnitude of isotopic alteration is reduced as solid and aqueous components approach equilibrium; however, rates of stable mineral recrystallization ($\sim 10^{-3}$ to 10^{-20} cm^2 s^{-1}; Gallagher et al. (1968); Tang et al. (2003); Gorski and Fantle (2017)) can exceed those expected for solid state diffusion at ~100°C by orders of magnitude ($\sim 10^{-20}$ to 10^{-43} cm^2 s^{-1}; Lahav and Bolt (1964); Kronenberg et al. (1984)) without overt changes to the mineral structure, elemental composition, or grain size even when the isotopic system is near equilibrium (e.g. Fantle (2015)). For this reason, stable mineral recrystallization is favored as a plausible late-stage alteration mechanism for the Jialazi Fm in the near-surface, and has potential implications elsewhere in the terrestrial carbonate record.

6. Interpreting carbonate alteration from clumped isotope-derived thermal histories

Previous investigations of material-specific (e.g. cements vs. brachiopods vs. micrite) bulk and clumped isotope compositions of buried sedimentary carbonates have found similar diagenetic behaviors: namely, that moderate burial induces significant but differential recrystallization based on material-specific parameters under largely rock-buffered settings on the prograde path (Shen-

ton et al., 2015; Lawson et al., 2018; Lacroix and Niemi, 2019). Fabrics and isotopic compositions from prograde crystallization, including ~70 to 80°C of $T(\Delta_{47})$ variability, are preserved throughout exhumation in each of these carbonate sequences. Using analogous techniques in the Jialazi Fm, which reached comparable burial depths, I find fundamentally different alteration behavior. For example, although textural observations are indicative of rock-buffered alteration, the oxygen isotopic compositions require that open system exchange occurred at some point during the burial history of the Jialazi Fm. As such, it is reasonable to believe that other sedimentary sections that have reached similar burial depths could have experienced fabric retentive, open-system water-rock alteration that has previously been interpreted as a closed-system retaining primary isotopic compositions.

Further, although the Jialazi Fm also yields a similar magnitude of $T(\Delta_{47})$ variability, the post-exhumation, low $T(\Delta_{47})$ values distinguish our findings from those of other basins. Shenton et al. (2015) interpret one $T(\Delta_{47})$ of ~21°C as late-stage void-filling cementation, but do not use this secondary calcite $T(\Delta_{47})$ within any alteration history plots or modeling, nor do they consider the implications of this type of recrystallization within the context of the broader carbonate record. We are able to make a unique interpretation of the diagenetic setting of carbonates that yield low $T(\Delta_{47})$ because we have eliminated all other possibilities through modeling efforts informed by isotopic measurements (Fig. 10). Therefore, the deduction of a post-exhumation, low-temperature alteration event sets the present work apart from past clumped isotope studies of thermal alteration histories.

Consistent with the findings of the present study, Lacroix and Niemi (2019) also demonstrate that CL petrography and stable isotope measurements alone are insufficient for identifying the degree of alteration, particularly in micritic carbonates. Instead, additional tools are required for identifying alteration processes beyond fabric retentive alteration during deeper burial diagenesis (Snell et al., 2013; Lacroix and Niemi, 2019).

7. Significance for paleoclimate and tectonic applications

The use of carbonate clumped isotope thermometry in reconstructing ancient environments requires preservation of primary ^{13}C–^{18}O bond ordering, and a reliable means of identifying diagenetic overprinting of the depositional Δ_{47} value. However, two sets of isotopic results are cause for concern for the continued use of carbonate clumped isotopes in orogenic settings: (1) the low T(Δ_{47}) values after burial to the solid-state reordering threshold for 10s of millions of years (Stolper and Eiler, 2015; Orme, 2017) and complete alteration of $\delta^{18}O$; and, (2) the alteration of marine carbonate from ∼–2‰ VPDB to ∼–14 to –22‰ VPDB without identifiable bulk recrystallized calcite domains and observed preservation of internal biogenic carbonate structures (e.g. cross-lamellar fabric, foram test porosity).

Importantly, the $\delta^{18}O$ and Δ_{47} compositions of the low-T Jialazi Fm samples are identical with the compositions and formation temperatures of modern lacustrine and pedogenic carbonates formed at >4 km elevation on the Tibetan Plateau. Because of the extreme disparity between water composition in the depositional (shallow marine) and modern alteration setting, $\delta^{18}O_c$ alteration was easy to identify in the absence of clear petrographic evidence. However, without a ground-truthing value such as marine $\delta^{18}O_w$, the low T(Δ_{47}) values in conjunction with low $\delta^{18}O_c$ values and preserved primary textures in terrestrial carbonates could be interpreted as a record of carbonate formation in a high-altitude environment such as the modern Tibetan Plateau. In light of these observations, it is necessary to reconsider interpretations of carbonate clumped isotope results in past studies orogenic basins. For example, T(Δ_{47}) values of pedogenic and lacustrine carbonates from the Penbo basin (SE Tibet), of a similar age and latitude as the Jialazi Fm, were used with oxygen isotope paleoaltimetry to reconstruct Paleocene-Eocene land surface elevations of the Linzizhong volcanic arc just prior to the India-Asia collision (Ingalls et al., 2017b). Although Ingalls et al. (2017b) used careful petrography to differentiate primary and altered carbonate fabrics, the present study has demonstrated

that texturally cryptic, late-stage alteration can yield low T(Δ_{47}) values reflecting secondary carbonate formation during or post-exhumation after prior water-rock exchange has overprinted the depositional $\delta^{18}O_c$ value. This is just one example of many in which petrography was the main method of diagenetic screening when using carbonate clumped isotopes in tectonic applications. Unlike in marine systems for which we have good constraints on starting compositions, in studies reconstructing ancient terrestrial environments, there are no ground-truthing isotopic values from which to ascertain $\delta^{18}O_c$ alteration. Therefore, we cannot currently prove or disprove standing interpretations of past clumped isotope results from terrestrial systems, but where possible, it is helpful to construct a paleo-environmental or tectonic model using multiple isotopic proxies or carbonate mineralogies with unique susceptibilities to alteration (e.g. Polissar et al. (2009); Currie et al. (2016); Ingalls et al. (2017a)).

8. Conclusions

Carbonate rocks hold many of the details of past climate states, which in turn reflect the behavior of climate-tectonic feedbacks and dynamics. A complete understanding of how and when 'clumped' isotopes reorder during burial and exhumation is imperative for the robust use of Δ_{47} in certain Earth science applications. Paired models of water-rock exchange and solid-state reordering allow us to better understand the conditions under which carbonates have altered in buried sedimentary basins.

In the Tso Jianding Group, the extensively altered $\delta^{18}O$ and intra-sample variability in Δ_{47} is contradicted by the preservation of depositional carbonate fabrics and fossil morphologies. Water-rock isotopic exchange reactions and solid-state reordering models are used to calculate the expected isotopic compositions of carbonate altered with a range of plausible diagenetic fluid compostions and under different W:R and temperature conditions based on previously published time-temperature histories. From the model results and stable isotope measurements, the following alteration history is determined (Fig. 10): (1) shal-

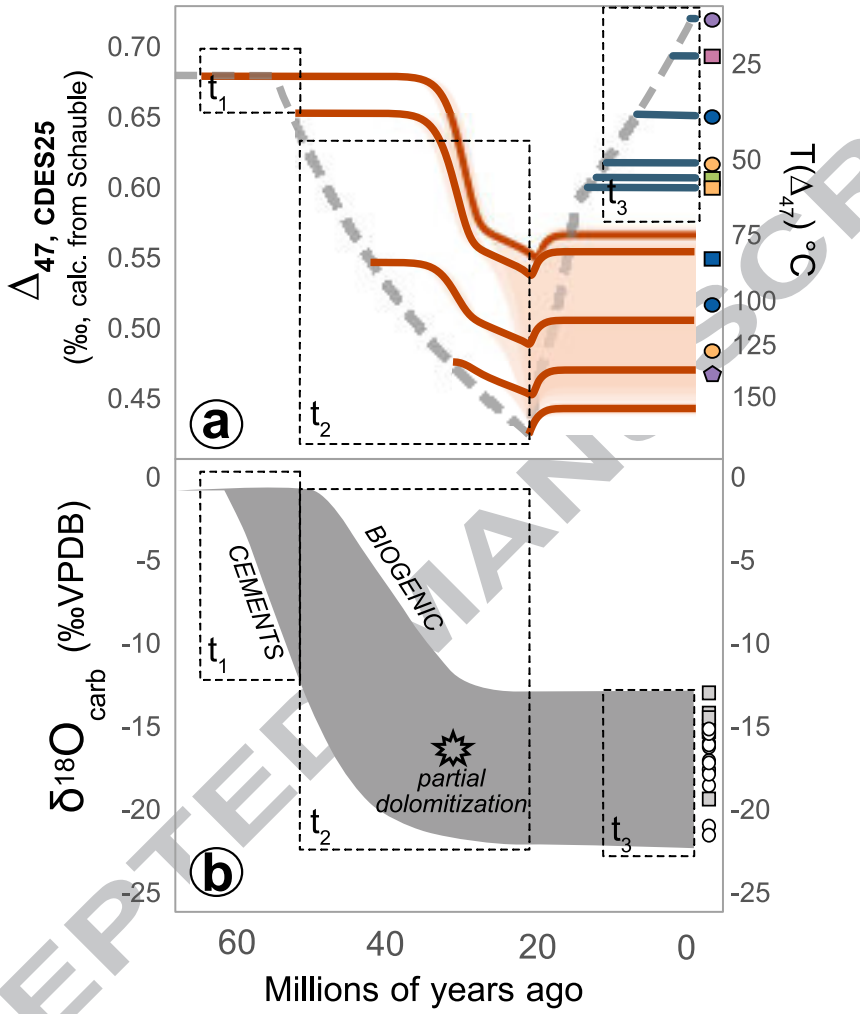

Figure 10: **Proposed carbonate alteration history of the Jialazi Fm, Xigaze forearc, S. Tibet, in three steps:** t_1: Microspar cementation, early marine diagenesis, and shallow burial alteration; t_2: Pervasive, high-T, variable W:R Δ_{47} and $\delta^{18}O_c$ alteration, and partial solid-state reordering; t_3 Low-T differential Δ_{47} alteration with minimal $\delta^{18}O_c$ change. Textures are preserved through all stages. **A.** Δ_{47} evolution by recrystallization followed by solid-state reordering in t_2 (red) and variable, low-temperature recrystallization in t_3. **B.** Range of potential $\delta^{18}O_c$ through the time-temperature history given the model results. Timing and composition of partial dolomitization (T0702-4) is noted. Biogenic (circles) and cement (squares) carbonates label the extremes of the composition envelope because higher $\delta^{18}O$ values were more characteristic of the biogenic carbonates (data plotted at 0Ma).

low, early diagenesis with water of similar composition and temperature to formation waters infills primary porespace with microspar; (2) high-temperature, rock-buffered water-rock exchange and partial solid-state reordering at >3-4 km depth; and (3) near-surface, low-temperature water-rock exchange on the exhumation pathway. A low-temperature and texturally preservative mechanism, such as stable mineral recrystallization, may explain some cases of intra-sample geochemical heterogeneity and stratigraphic isotopic variability in other sedimentary sections in the absence of a global isotopic excursion.

An important finding of this work is that carbonate are interpreted to have experienced significant low-temperature alteration in the shallow subsurface or in outcrop with minimal textural evidence of material exchange, which has significant implications for interpretations of stable isotopic compositions of carbonate rocks for many applications. A more complete understanding of low-temperature carbonate alteration mechanisms and how this type of alteration can be identified is essential for the robust use of carbonate-derived proxies from exhumed orogenic sedimentary basins in paleoclimate and tectonics studies. Existing low T(Δ_{47}) results screened for alteration by petrography alone may require reassessment as we improve our understanding of near-surface carbonate alteration and its pervasiveness in the sedimentary record.

Acknowledgements

MI would like to thank David Rowley and Albert Colman for use of analytical facilities and a great deal of discussion leading to this work, and Brian Currie for assistance with cathodoluminescence imaging. MI thanks Madison Ball for his assistance in the field, and Xu Qiang and Ding Lin for coordination of field logistics in China. MI would also like to thank Devon Orme for discussion of the thermal history of the Xigaze forearc during the development of this work and openness in data sharing prior to publication, Max Lloyd for sharing early versions of reordering models and dolomite reordering kinetics, and Daniel Stolper for discussions of reordering and carbonate diagenesis. Funding for

this work was provided by a Geological Society of America Graduate Student Research Grant to MI, Sigma Xi Grants-in-Aid G2016100187643997 to MI, and NSF EAR grants 1111274 to David Rowley and 0923831 to David Rowley and Albert Colman.

References

Ahm, A. S. C., Bjerrum, C. J., Blättler, C. L., Swart, P. K., Higgins, J. A., 2018. Quantifying early marine diagenesis in shallow-water carbonate sediments. Geochimica et Cosmochimica Acta.

Aitchison, J. C., Xia, X., Baxter, A. T., Ali, J. R., 2011. Detrital zircon U-Pb ages along the Yarlung-Tsangpo suture zone, Tibet: Implications for oblique convergence and collision between India and Asia. Gondwana Research 20 (4), 691–709.

Avrahamov, N., Sivan, O., Yechieli, Y., Lazar, B., 2013. Carbon Isotope Exchange During Calcite Interaction With Brine : implications for 14C dating of Hypersaline Groundwater. Radiocarbon 55 (1), 81–101.

Banner, J. L., Hanson, G. N., nov 1990. Calculation of simultaneous isotopic and trace element variations during water-rock interaction with applications to carbonate diagenesis. Geochimica et Cosmochimica Acta 54 (11), 3123–3137.

Barnaby, R. J., Rimstidt, J. D., 1989. Redox conditions of calcite cementation interpreted from Mn and Fe contents of authigenic calcites. Geological Society of America Bulletin.

Bergman, S. C., Huntington, K. W., Crider, J. G., 2013. Tracing paleofluid sources using clumped isotope thermometry of diagenetic cements along the moab fault, Utah. American Journal of Science 313 (5), 490–515.

Bershaw, J., Penny, S., Garzione, C. N., 2012. Stable isotopes of modern water across the Himalaya and eastern Tibetan Plateau: Implications for estimates of paleoelevation and paleoclimate. Journal of Geophysical Research 117 (D2).

Boggs, S., Krinsley, D., 2006. Application of Cathodoluminescence Imaging to the Study of Sedimentary Rocks. Cambridge University Press.

Bouilhol, P., Jagoutz, O., Hanchar, J. M., Dudas, F. O., 2013. Dating the India-Eurasia collision through arc magmatic records. Earth and Planetary Science Letters 366, 163–175.

Budd, D. A., Pack, S. M., Fogel, M. L., 2002. The destruction of paleoclimatic isotopic signals in Pleistocene carbonate soil nodules of Western Australia. Palaeogeography, Palaeoclimatology, Palaeoecology 188 (3-4), 249–273.

Carrapa, B., Orme, D. A., DeCelles, P. G., Kapp, P., Cosca, M. A., Waldrip, R., 2014. Miocene burial and exhumation of the India-Asia collision zone in southern Tibet: Response to slab dynamics and erosion. Geology.

Choquette, P. W., Pray, L. C., 1970. Geologic nomenclatures and classification of porosity in sedimentary carbonates. AAPG Bulletin 54 (2), 207–250.

Chung, S. L., Chu, M. F., Zhang, Y., Xie, Y., Lo, C. H., Lee, T. Y., Lan, C. Y., Li, X., Zhang, Q., Wang, Y., 2005. Tibetan tectonic evolution inferred from spatial and temporal variations in post-collisional magmatism. Earth-Science Reviews 68 (3-4), 173–196.

Cummins, R. C., Finnegan, S., Fike, D. A., Eiler, J. M., Fischer, W. W., 2014. Carbonate clumped isotope constraints on Silurian ocean temperature and seawater ??18O. Geochimica et Cosmochimica Acta 140, 241–258.
URL http://dx.doi.org/10.1016/j.gca.2014.05.024

Currie, B. S., Polissar, P. J., Rowley, D. B., Ingalls, M., Li, S., Freeman, K. H., 2016. Multiproxy paleoaltimetry of the late Oligocene-Pliocene Oiyug Basin, southern Tibet. American Journal of Science 316 (5), 401–436.

763 Curti, E., Fujiwara, K., Iijima, K., Tits, J., Cuesta, C., Kitamura, A., Glaus,
764 M. A., Müller, W., 2010. Radium uptake during barite recrystallization at
765 232C as a function of solution composition: An experimental 133Ba and
766 226Ra tracer study. Geochimica et Cosmochimica Acta 74 (12), 3553–3570.

767 Dale, A., John, C. M., Mozley, P. S., Smalley, P. C., Muggeridge, A. H., 2014.
768 Time-capsule concretions: Unlocking burial diagenetic processes in the Man-
769 cos Shale using carbonate clumped isotopes. Earth and Planetary Science
770 Letters 394, 30–37.

771 DeCelles, P., Kapp, P., Gehrels, G., Ding, L., 2014. PaleoceneEocene foreland
772 basin evolution in the Himalaya of southern Tibet and Nepal: Implications
773 for the age of initial IndiaAsia collision. Tectonics 33.

774 Defliese, W. F., Lohmann, K. C., 2015. Non-linear mixing effects on mass-
775 47 CO2 clumped isotope thermometry: Patterns and implications. Rapid
776 Communications in Mass Spectrometry 29 (9), 901–909.

777 Dennis, K., Affek, H., Passey, B., Schrag, D., Eiler, J., 2011. Defining an ab-
778 solute reference frame for 'clumped' isotope studies of CO2. Geochimica et
779 Cosmochimica Acta 75 (22), 7117–7131.

780 Dennis, K. J., Schrag, D. P., jul 2010. Clumped isotope thermometry of carbon-
781 atites as an indicator of diagenetic alteration. Geochimica et Cosmochimica
782 Acta 74 (14), 4110–4122.

783 Ding, L., Kapp, P., Wan, X., jun 2005. Paleocene-Eocene record of ophiolite ob-
784 duction and initial India-Asia collision, south central Tibet. Tectonics 24 (3).

785 Dodson, M. H., 1973. Closure temperature in cooling geochronological and
786 petrological systems. Contributions to Mineralogy and Petrology 40 (3), 259–
787 274.

788 Eagle, R. A., Schauble, E. A., Tripati, A. K., Tütken, T., Hulbert, R. C., Eiler,
789 J. M., 2010. Body temperatures of modern and extinct vertebrates from 13C-

18O bond abundances in bioapatite. Proceedings of the National Academy of Sciences 107 (23), 10377–10382.

Eiler, J. M., 2007. Clumped-isotope geochemistryThe study of naturally-occurring, multiply-substituted isotopologues. Earth and Planetary Science Letters 262 (3-4), 309–327.

Eiler, J. M., 2011. Paleoclimate reconstruction using carbonate clumped isotope thermometry. Quaternary Science Reviews 30 (25), 3575–3588.

Einsele, G., Liu, B., Dürr, S., Frisch, W., Liu, G., Luterbacher, H. P., Ratschbacher, L., Ricken, W., Wendt, J., Wetzel, A., Yu, G., Zheng, H., 1994. The Xigaze forearc basin: evolution and facies architecture (Cretaceous, Tibet). Sedimentary Geology 90 (1-2), 1–32.

Fantle, M. S., 2015. Calcium isotopic evidence for rapid recrystallization of bulk marine carbonates and implications for geochemical proxies. Geochimica et Cosmochimica Acta 148, 378–401.

Fantle, M. S., Higgins, J., 2014. The effects of diagenesis and dolomitization on Ca and Mg isotopes in marine platform carbonates: Implications for the geochemical cycles of Ca and Mg. Geochimica et Cosmochimica Acta 142, 458–481.

Faÿ-Gomord, O., Allanic, C., Verbiest, M., Honlet, R., Champenois, F., Bonifacie, M., Chaduteau, C., Wouters, S., Muchez, P., Lasseur, E., Swennen, R., 2018. Understanding fluid flow during tectonic reactivation: An example from the Flamborough head chalk outcrop (UK). Geofluids 2018, 17.

Fernandez, A., Müller, I. A., Rodríguez-Sanz, L., van Dijk, J., Looser, N., Bernasconi, S. M., 2017. A Reassessment of the Precision of Carbonate Clumped Isotope Measurements: Implications for Calibrations and Paleoclimate Reconstructions. Geochemistry, Geophysics, Geosystems 18 (12), 4375–4386.

817 Fernandez, A., Tang, J., Rosenheim, B. E., 2014. Siderite clumped' isotope
818 thermometry: A new paleoclimate proxy for humid continental environments.
819 Geochimica et Cosmochimica Acta 126, 411–421.

820 Frierdich, A. J., Catalano, J. G., 2012. Controls on Fe(II)-activated trace ele-
821 ment release from goethite and hematite. Environmental Science and Tech-
822 nology 46 (3), 1519–1526.

823 Gallagher, K. J., Feitknecht, W., Mannweiler, U., 1968. Mechanism of oxidation
824 of magnetite to γ-Fe2O3. Nature.

825 Garzione, C. N., Dettman, D. L., Quade, J., DeCelles, P. G., Butler, R., 2000.
826 High times on the Tibetan Plateau: Paleoelevation of the Thakkhola graben,
827 Nepal. Geology 28, 339–342.

828 Ghosh, P., Adkins, J., Affek, H., Balta, B., Guo, W. W., Schauble, E. E. a.,
829 Schrag, D., Eller, J., Eiler, J. M., 2006a. 13C-18O bonds in carbonate min-
830 erals: A new kind of paleothermometer. Geochimica et Cosmochimica Acta
831 70 (6), 1439–1456.

832 Ghosh, P., Garzione, C. N., Eiler, J. M., 2006b. Rapid uplift of the Altiplano
833 revealed through 13C-18O bonds in paleosol carbonates. Science (New York,
834 N.Y.) 311 (5760), 511–5.

835 Gorski, C. A., Fantle, M. S., 2017. Stable mineral recrystallization in low tem-
836 perature aqueous systems: A critical review. Geochimica et Cosmochimica
837 Acta 198, 439–465.

838 Guo, W., Mosenfelder, J. L., Goddard, W. A., Eiler, J. M., 2009. Isotopic frac-
839 tionations associated with phosphoric acid digestion of carbonate minerals:
840 Insights from first-principles theoretical modeling and clumped isotope mea-
841 surements. Geochimica et Cosmochimica Acta 73 (24), 7203–7225.

842 Handler, R. M., Beard, B. L., Johnson, C. M., Scherer, M. M., 2009. Atom
843 exchange between aqueous Fe(II) and goethite: An Fe isotope tracer study.
844 Environmental Science and Technology 43 (4), 1102–1107.

Handler, R. M., Frierdich, A. J., Johnson, C. M., Rosso, K. M., Beard, B. L., Wang, C., Latta, D. E., Neumann, A., Pasakarnis, T., Premaratne, W. A., Scherer, M. M., 2014. Fe(II)-catalyzed recrystallization of goethite revisited. Environmental Science and Technology 48 (19), 11302–11311.

He, B., Olack, G., Colman, A., 2012. Pressure baseline correction and high-precision CO2 clumped-isotope (47) measurements in bellows and micro-volume modes. Rapid Communications in Mass Spectrometry 26 (24), 2837–53.

He, S., Kapp, P., DeCelles, P. G., Gehrels, G. E., Heizler, M., 2007. Cretaceous-Tertiary geology of the Gangdese Arc in the Linzhou area, southern Tibet. Tectonophysics.

Henkes, G. A., Passey, B. H., Grossman, E. L., Shenton, B. J., Perez-Huerta, A., Yancey, T. E., 2014. Temperature limits for preservation of primary calcite clumped isotope paleotemperatures. Geochimica et Cosmochimica Acta 139, 362–382.

Henkes, G. A., Passey, B. H., Wanamaker, A. D., Grossman, E. L., Ambrose, W. G., Carroll, M. L., 2013. Carbonate clumped isotope compositions of modern marine mollusk and brachiopod shells. Geochimica et Cosmochimica Acta 106, 307–325.

Higgins, J. A., Blättler, C. L., Lundstrom, E. A., Santiago-Ramos, D. P., Akhtar, A. A., Crüger Ahm, A. S., Bialik, O., Holmden, C., Bradbury, H., Murray, S. T., Swart, P. K., 2018. Mineralogy, early marine diagenesis, and the chemistry of shallow-water carbonate sediments. Geochimica et Cosmochimica Acta 220, 512–534.

Hren, M., Bookhagen, B., Blisniuk, P., Booth, A., Chamberlain, C., 2009. d18O and dD of streamwaters across the Himalaya and Tibetan Plateau: Implications for moisure sources and paleoelevation reconstructions. Earth and Planetary Science Letters 288, 20–32.

Hu, X., Garzanti, E., Moore, T., Raffi, I., 2015. Direct stratigraphic dating of India-Asia collision onset at the Selandian (middle Paleocene, 59 +- 1 Ma). Geology 43 (10), 859–862.

Hu, X., Wang, J., BouDagher-Fadel, M., Garzanti, E., An, W., 2016. New insights into the timing of the India-Asia collision from the Paleogene Quxia and Jialazi formations of the Xigaze forearc basin, South Tibet. Gondwana Research 32, 76–92.

Huntington, K. W., Budd, D. A., Wernicke, B. P., Eiler, J. M., 2011. Use of clumped-isotope thermometry to constrain the crystallization temperature of diagenetic calcite. Journal of Sedimentary Research 81 (9), 656–669.

Huntington, K. W., Saylor, J., Quade, J., Hudson, A. M., 2015. High late Miocene-Pliocene elevation of the Zhada Basin, southwestern Tibetan Plateau, from carbonate clumped isotope thermometry. Geological Society of America Bulletin 127 (1-2), 181–199.

Ingalls, M., Rowley, D., Olack, G., Currie, B., Li, S., Schmidt, J., Tremblay, M., Polissar, P., Shuster, D., Lin, D., Colman, A., 2017a. Paleocene to Pliocene low-latitude, high-elevation basins of southern Tibet: Implications for tectonic models of India-Asia collision, Cenozoic climate, and geochemical weathering. Bulletin of the Geological Society of America 130 (1-2).

Ingalls, M., Rowley, D. B., Olack, G., Currie, B. S., Li, S., Schmidt, J., Tremblay, M., Polissar, P. J., Shuster, D. L., Lin, D., Colman, A. S., 2017b. Paleocene to Pliocene low-latitude, high-elevation basins of southern Tibet: Implications for tectonic models of India-Asia collision, Cenozoic climate, and geochemical weathering. Geological Society of America Bulletin 130 (1-2), 307–330.

Ivany, L., Lohmann, K. C., Patterson, W., 2003. Paleogene Temperature History of the U.S. Gulf Coastal Plain Inferred from d18O of Fossil Otoliths. In: From Greenhouse to Icehouse: The Marine Eocene-Oligocene Transition. pp. 232–251.

Katz, A., Bonifacie, M., Hermoso, M., Cartigny, P., Calmels, D., 2017. Laboratory-grown coccoliths exhibit no vital effect in clumped isotope (Δ47) composition on a range of geologically relevant temperatures. Geochimica et Cosmochimica Acta 208, 335–353.

Keating-Bitonti, C. R., Ivany, L. C., Affek, H. P., Douglas, P., Samson, S. D., 2011. Warm, not super-hot, temperatures in the early Eocene subtropics. Geology 39 (8), 771–774.

Kele, S., Breitenbach, S. F., Capezzuoli, E., Meckler, A. N., Ziegler, M., Millan, I. M., Kluge, T., Deák, J., Hanselmann, K., John, C. M., Yan, H., Liu, Z., Bernasconi, S. M., 2015. Temperature dependence of oxygen- and clumped isotope fractionation in carbonates: A study of travertines and tufas in the 6-95 C temperature range. Geochimica et Cosmochimica Acta 168, 172–192.

Kim, S.-T., O'Neil, J. R., 1997. Equilibrium and nonequilibrium oxygen isotope effects in synthetic carbonates. Geochimica et Cosmochimica Acta 61 (16), 3461–3475.

Kobashi, T., Grossman, E. L., Yancey, T. E., Dockery, D. T., 2001. Reevaluation of conflicting Eocene tropical temperature estimates: Molluskan oxygen isotope evidence for warm low latitudes. Geology 29 (11), 983–986.

Kronenberg, A. K., Yund, R. A., Giletti, B. J., 1984. Carbon and oxygen diffusion in calcite: Effects of Mn content and PH2O. Physics and Chemistry of Minerals.

Lacroix, B., Niemi, N. A., 2019. Investigating the effect of burial histories on the clumped isotope thermometer: An example from the Green River and Washakie Basins, Wyoming. Geochimica et Cosmochimica Acta 247, 40–58. URL https://www.sciencedirect.com/science/article/pii/S001670371830704X

Lahav, N., Bolt, G. H., 1964. Self-diffusion of Ca45 into certain carbonates. Soil Science.

Lawson, M., Shenton, B. J., Stolper, D. A., Eiler, J. M., Rasbury, E. T., Becker, T. P., Phillips-Lander, C. M., Buono, A. S., Becker, S. P., Pottorf, R., Gray, G. G., Yurewicz, D., Gournay, J., 2018. Deciphering the diagenetic history of the El Abra Formation of eastern Mexico using reordered clumped isotope temperatures and U-Pb dating. Bulletin of the Geological Society of America 130 (3-4), 617–629.

Leary, R., Orme, D. A., Laskowski, A. K., DeCelles, P. G., Kapp, P., Carrapa, B., Dettinger, M., 2016. Along-strike diachroneity in deposition of the Kailas Formation in central southern Tibet: Implications for Indian slab dynamics. Geosphere 12 (4), 1198–1223.

Lee, H. Y., Chung, S. L., Lo, C. H., Ji, J., Lee, T. Y., Qian, Q., Zhang, Q., 2009. Eocene Neotethyan slab breakoff in southern Tibet inferred from the Linzizong volcanic record. Tectonophysics 477 (1-2), 20–35.

Lestini, L., Beaucaire, C., Vercouter, T., Descostes, M., 2013. Radium Uptake by Recrystallized Gypsum: An Incorporation Study. Procedia Earth and Planetary Science 7, 479–482.

Lloyd, M., Ryb, U., Eiler, J., 2018. Experimental determination of the preservation potential of the dolomite clumped isotope thermometer. Geochimica et Cosmochimica Acta 242, 1–20.

Mangenot, X., Gasparrini, M., Rouchon, V., Bonifacie, M., 2018. Basin-scale thermal and fluid flow histories revealed by carbonate clumped isotopes ($\Delta 47$) Middle Jurassic carbonates of the Paris Basin depocentre. Sedimentology.

Marshall, D. J., 1988. Cathodoluminescence of Geological Materials. Unwin Hyman Boston etc., Boston.

Miller, K. G., Fairbanks, R. G., Mountain, G. S., 1987. Tertiary oxygen isotope synthesis, sea level history, and continental margin erosion. Paleoceanography 2 (1), 1–19.

Munnecke, A., Westphal, H., Reijmer, J. J. G., Samtleben, C., 1997. Microspar development during early marine burial diagenesis: A comparison of Pliocene carbonates from the Bahamas with Silurian limestones from Gotland (Sweden). Sedimentology 44 (6), 977–990.

Orme, D. A., 2017. Burial and exhumation history of the Xigaze forearc basin, Yarlung suture zone, Tibet. Geoscience Frontiers (Himalaya Special Issue), 1–15.

Orme, D. A., Carrapa, B., Kapp, P., 2014. Sedimentology, provenance and geochronology of the upper Cretaceous-lower Eocene western Xigaze forearc basin, southern Tibet. Basin Research 27, 387–411.

Orme, D. A., Laskowski, A. K., 2016. Basin Analysis of the Albian Santonian Xigaze Forearc , Lazi Region , South-Central Tibet. Journal of Sedimentary Research 86 (August), 894–913.

Passey, B. H., Henkes, G. A., 2012. Carbonate clumped isotope bond reordering and geospeedometry. Earth and Planetary Science Letters 351-352, 223–236.

Passey, B. H., Levin, N. E., Cerling, T. E., Brown, F. H., Eiler, J. M., 2010. High-temperature environments of human evolution in East Africa based on bond ordering in paleosol carbonates. Proceedings of the National Academy of Sciences of the United States of America 107 (25), 11245–9.

Polissar, P. J., Freeman, K. H., Rowley, D. B., McInerney, F. a., Currie, B. S., sep 2009. Paleoaltimetry of the Tibetan Plateau from D/H ratios of lipid biomarkers. Earth and Planetary Science Letters 287 (1-2), 64–76.
URL http://linkinghub.elsevier.com/retrieve/pii/S0012821X09004531http://www.sciencedirect.com/science/article/pii/S0012821X09004531

Quade, J., Breecker, D. O., Daeron, M., Eiler, J. M., 2011. The paleoaltimetry of Tibet: An isotopic perspective. American Journal of Science 311 (2), 77–115.

Region, B., 1993. Regional Geology of Xizang (Tibet) Autonomous Region, Beijing.

Schärer, U., Xu, R. H., Allègre, C. J., 1984. U/Pb geochronology of Gangdese (Transhimalaya) plutonism in the Lhasa-Xigaze region, Tibet. Earth and Planetary Science Letters.

Schauble, E. A., Ghosh, P., Eiler, J. M., 2006. Preferential formation of 13C-18O bonds in carbonate minerals, estimated using first-principles lattice dynamics. Geochimica et Cosmochimica Acta 70 (10), 2510–2529.

Shenton, B. J., Grossman, E. L., Passey, B. H., Henkes, G. A., Becker, T. P., Laya, J. C., Perez-Huerta, A., Becker, S. P., Lawson, M., 2015. Clumped isotope thermometry in deeply buried sedimentary carbonates: The effects of bond reordering and recrystallization. Bulletin of the Geological Society of America 127 (7-8), 1036–1051.

Snell, K. E., Koch, P. L., Druschke, P., Foreman, B. Z., Eiler, J. M., 2014. High elevation of the 'Nevadaplano' during the Late Cretaceous. Earth and Planetary Science Letters 386, 52–63.

Snell, K. E., Thrasher, B. L., Eiler, J. M., Koch, P. L., Sloan, L. C., Tabor, N. J., 2013. Hot summers in the Bighorn Basin during the early Paleogene. Geology 41 (1), 55–58.

Solomon, S., Walkden, G., 1985. the Application of Cathodoluminescence To Interpreting the Diagenesis of an Ancient Calcrete Profile. Sedimentology 32 (6), 877–896.

Sommer, S. E., 1972. Cathodoluminescence of carbonates, 1. Characterization of cathodoluminescence from carbonate solid solutions. Chemical Geology.

Spooner, P. T., Guo, W., Robinson, L. F., Thiagarajan, N., Hendry, K. R., Rosenheim, B. E., Leng, M. J., 2016. Clumped isotope composition of cold-water corals: A role for vital effects? Geochimica et Cosmochimica Acta 179, 123–141.

Stipp, S. L., Hochella, M. F., Parks, G. A., Leckie, J. O., 1992. Cd2+uptake by calcite, solid-state diffusion, and the formation of solid-solution: Interface processes observed with near-surface sensitive techniques (XPS, LEED, and AES). Geochimica et Cosmochimica Acta 56 (5), 1941–1954.

Stolper, D. A., Eiler, J. M., 2015. The kinetics of solid-state isotope-exchange reactions for clumped isotopes: A study of inorganic calcites and apatites from natural and experimental samples. American Journal of Science 315 (5), 363–411.

Stolper, D. A., Eiler, J. M., Higgins, J. A., 2018. Modeling the effects of diagenesis on carbonate clumped-isotope values in deep- and shallow-water settings. Geochimica et Cosmochimica Acta 227, 264–291.

Swart, P. K., Burns, S. J., Leder, J. J., 1991. Fractionation of the stable isotopes of oxygen and carbon in carbon dioxide during the reaction of calcite with phosphoric acid as a function of temperature and technique. Chemical Geology: Isotope Geoscience Section.

Swart, P. K., Cantrell, D. L., Arienzo, M. M., Murray, S. T., 2016. Evidence for high temperature and 18O-enriched fluids in the Arab-D of the ghawar field, Saudi Arabia. Sedimentology 63 (6), 1739–1752.

Tang, J., Myers, M., Bosnick, K. A., Brus, L. E., 2003. Magnetite Fe3O4 Nanocrystals: Spectroscopic Observation of Aqueous Oxidation Kinetics. J. Phys. Chem. B.

VanDeVelde, J. H., Bowen, G. J., Passey, B. H., Bowen, B. B., 2013. Climatic and diagenetic signals in the stable isotope geochemistry of dolomitic paleosols spanning the Paleocene-Eocene boundary. Geochimica et Cosmochimica Acta 109, 254–267.

Wachter, E. A., Hayes, J. M., 1985. Exchange of oxygen isotopes in carbon dioxide-phosporic acid systems. Chemical Geology: Isotope Geoscience Section.

Wan, X., Wang, L., Wang, C., Luba, J., 1998. Discovery and significance of Cretaceous fossils from the Xigaze Forearc Basin, Tibet. Journal of Asian Earth Sciences 16 (2), 217–223.

Wang, C., Li, X., Liu, Z., Li, Y., Jansa, L., Dai, J., Wei, Y., 2012. Revision of the Cretaceous-Paleogene stratigraphic framework, facies architecture and provenance of the Xigaze forearc basin along the Yarlung Zangbo suture zone. Gondwana Research 22 (2), 415–433.

Wang, J., Hu, X., Jansa, L., Huang, Z., 2011. Provenance of the Upper CretaceousEocene Deep-Water Sandstones in Sangdanlin, Southern Tibet: Constraints on the Timing of Initial India-Asia Collision. The Journal of Geology 119 (3), 293–309.

Wen, D. R., Liu, D., Chung, S. L., Chu, M. F., Ji, J., Zhang, Q., Song, B., Lee, T. Y., Yeh, M. W., Lo, C. H., 2008. Zircon SHRIMP U-Pb ages of the Gangdese Batholith and implications for Neotethyan subduction in southern Tibet. Chemical Geology 252 (3-4), 191–201.

Winkelstern, I. Z., Lohmann, K. C., 2016. Shallow burial alteration of dolomite and limestone clumped isotope geochemistry. Geology 44 (6), 467–470.

Yin, A., Harrison, T. M., 2000. Geologic evolution of the Himalayan - Tibetan orogen. Annual Review 28, 211–280.

Zaarur, S., Affek, H. P., Brandon, M. T., 2013. A revised calibration of the clumped isotope thermometer. Earth and Planetary Science Letters 382, 47–57.

Zaarur, S., Olack, G., Affek, H. P., 2011. Paleo-environmental implication of clumped isotopes in land snail shells. Geochimica et Cosmochimica Acta 75 (22), 6859–6869.

Appendix A Tables

ACCEPTED MANUSCRIPT

Table S1: **Lithologies, sample locations, and carbon and oxygen stable isotope data for the Tso Jiangding.**

Sample	Lithology	Orme et al. (2014) Section	Latitude (°N)	Longitude (°E)	$\delta^{18}O_c$ ‰ VPDB	$\delta^{13}C$ ‰ VPDB	% CO_3^{2-}
T0702-2	fossiliferous floatstone	D/E - shallow marine	29.85989	84.84176	-16.2	-3.6	65
T0702-2Sh	shell	D/E - shallow marine	29.85989	84.84176	-15.3	-3.4	85
T0702-4	dolostone	D/E - shallow marine	29.85995	84.84175	-16.0	-3.1	86
T0702-4Sh	shell	D/E - shallow marine	29.85995	84.84175	-15.3	-2.5	14
T0702-6	fossiliferous floatstone	D/E - shallow marine	29.87528	84.84125	-20.9	-1.5	22
T0702-7	packstone	D/E - shallow marine	29.87533	84.84117	-21.4	-1.6	24
T0702-8	fossiliferous floatstone	D/E - shallow marine	29.87528	84.84125	-19.3	-1.0	17
T0702-8Sh	shell	D/E - shallow marine	29.87528	84.84125	-13.0	0.1	65
T0702-9	sandy limestone	D/E - shallow marine	29.87534	84.84115	-18.4	-1.0	17
T0702-10	fossiliferous floatstone	D/E - shallow marine	29.87536	84.84113	-17.5	0.6	18
T0702-11	sandy limestone	D/E - shallow marine	29.87537	84.84112	-17.5	-1.1	17
T0702-13	sandy limestone	D/E - shallow marine	29.87537	84.84112	-17.8	-1.6	12
T0702-14	packstone	D/E - shallow marine	29.87538	84.84109	-16.1	-1.5	7
T0702-14V	vein	D/E - shallow marine	29.87538	84.84109	-14.4	-2.1	47
T0702-16	limestone	D/E - shallow marine	29.87539	84.84107	-15.4	-1.0	26
T0702-17	limestone	D/E - shallow marine	29.87561	84.84075	-17.0	-1.1	9.5
T0702-18	fossiliferous packstone	D/E - shallow marine	29.87566	84.83996	-15.1	-0.3	42
T0702-18N1	foraminifera	D/E - shallow marine	29.87566	84.83996	-15.0	-0.3	31
T0702-19	packstone	D/E - shallow marine			-17.2	-1.7	13
T0702-19V	vein	D/E - shallow marine			-16.0	0.8	45
T0703-2	limestone	G/H - fluvial/deltaic	29.89091	84.74028	-29.5	-4.0	17
T0703-4v	vein within fluvial siltstone	G/H - fluvial/deltaic	29.88997	84.74184	-15.4	-7.5	68
T0703-7	limey sandstone	G/H - fluvial/deltaic	29.88947	84.74259	-22.4	-5.7	3
T0703-8	limey sandstone	G/H - fluvial/deltaic	29.88931	84.74213	-23.7	-6.0	9
T0703-9	quartz sand-rich paleosol	G/H - fluvial/deltaic	29.88942	84.74260	-22.9	-7.7	5
T0703-10	carbonate-rich paleosol	G/H - fluvial/deltaic	29.88942	84.74265	-21.7	-9.7	37
T0703-11	paleosol calcrete	G/H - fluvial/deltaic	29.88939	84.74271	-21.4	-8.7	2
T0703-12	paleosol calcrete	G/H - fluvial/deltaic	29.88938	84.74274	-24.2	-9.2	12
T0703-12V	vein	G/H - fluvial/deltaic	29.88938	84.74274	-16.9	-7.6	41
T0703-13	limey sandstone	G/H - fluvial/deltaic	29.88929	84.74279	-20.4	-8.6	2
T0703-16	paleosol; green	G/H - fluvial/deltaic	29.88915	84.74293	-0.4	-7.4	7
T0703-17	paleosol calcrete	G/H - fluvial/deltaic			-22.4	-6.9	12

Table S2: **All Δ_{47} measurements of Tso Jiangding Jialazi Fm samples.** The inferred oxygen isotopic composition of water in equilibrium with carbonate at measured Δ_{47}-derived temperatures is listed in the far right column. $*$ denotes measurements made on the MAT253. $\delta^{18}O_{CO_3}$ values were calculated using a CO_2-CO_3 acid fractionation factor (Guo et al., 2009).

					Inferred from T(Δ_{47})	
Sample	$\delta^{18}O^{*}_{CO_2}$ **VSMOW**	$\delta^{18}O_{CO_3}$ **VPDB**	$\Delta_{47}{}^{*}$	**T(Δ_{47}) °C**	$\alpha_{CO_3-H_2O}$	**equil. $\delta^{18}O_w$ VSMOW**
T0702-18	25.572	-15.192	0.536	74.9	1.01958	-4.235
T0702-18	24.735	-15.995	0.540	73.4	1.01980	-5.259
T0702-18	24.598	-16.127	0.563	65.2	1.02108	-6.649
T0702-18N1	25.085	-15.659	0.653	37.6	1.02593	-10.874
T0702-18N1	25.317	-15.436	0.641	40.9	1.02531	-10.047
T0702-18N2	26.335	-14.459	0.469	103.7	1.01555	0.458
T0702-18N2	26.204	-14.585	0.482	97.3	1.01638	-0.485
T0702-4	24.501	-16.220	0.460	108.1	1.01499	-0.779
T0702-4	24.663	-16.065	0.465	105.7	1.01529	-0.921
T0702-4	24.679	-16.049	0.456	110.0	1.01475	-0.368
T0702-4Sh	24.988	-15.752	0.721	20.7	1.02937	-14.271
T0702-6	19.407	-21.111	0.686	29.1	1.02761	-17.955
T0702-7	21.360	-19.236	0.613	50.0	1.02364	-12.385
T0702-7	21.236	-19.355	0.609	48.8	1.02385	-12.468
T0702-8	21.228	-19.363	0.589	72.3	1.01996	-9.149
T0702-8	20.896	-19.681	0.543	56.4	1.02254	-11.326
T0702-8	20.814	-19.761	0.688	28.4	1.02774	-16.730
T0702-8SH1	28.037	-12.825	0.467	104.6	1.01542	2.241
T0702-8SH2	26.493	-14.307	0.617	47.7	1.02406	-7.703
T0702-8SH2 recleaned	26.503	-14.297	0.621	46.7	1.02424	-7.873
T0702-8V	25.827	-14.946	0.524	79.8	1.01884	-3.265

Table S3: **All clumped isotope measurements run on standard materials during the analytical period in which Jialazi Fm measurements were made.**

Sample	δ^{13}**C**	$\delta^{18}\mathbf{O}_{CO_2}$	$\Delta_{47,SG-WG}$	δ_{47}	Δ_{48}	$\Delta_{47,CDES}$	**Analysis Date**
Carrara Marble	2.1	39.0	-0.511	19.0	0.246	0.402	9/11/15
	2.0	38.9	-0.518	18.8	1.147	0.395	9/29/15
	2.1	38.9	-0.476	18.9	0.741	0.440	9/29/15
	1.9	38.6	-0.501	18.5	1.114	0.412	9/30/15
	2.0	39.0	-0.521	18.9	1.177	0.392	10/6/15
	2.0	39.1	-0.525	19.0	0.882	0.388	10/14/15
	2.1	39.1	-0.564	19.0	-0.119	0.380	12/17/15
	2.0	39.0	-0.506	18.9	-0.737	0.438	1/12/16
	1.9	38.7	-0.466	18.5	-0.718	0.477	1/14/16
	2.0	39.0	-0.503	18.9	-0.645	0.441	1/25/16
	2.0	38.9	-0.513	18.8	-0.769	0.431	1/27/16
	1.9	38.7	-0.463	18.5	-1.283	0.481	1/27/16
	2.1	39.0	-0.502	19.0	0.517	0.442	3/16/16
	2.1	39.0	-0.505	19.0	0.454	0.439	3/16/16
	2.0	39.0	-0.504	19.0	0.392	0.440	4/6/16
	2.1	39.1	-0.508	19.1	0.468	0.437	4/13/16
	2.1	39.1	-0.495	19.0	0.407	0.449	4/21/16
	2.1	39.1	-0.483	19.1	0.108	0.461	4/27/16
	2.2	39.4	-0.492	19.5	0.439	0.454	5/26/16
	2.2	39.2	-0.459	19.4	0.689	0.486	5/30/16
	2.1	39.1	-0.497	19.0	0.247	0.448	7/7/16
	2.0	38.9	-0.531	18.8	0.169	0.413	7/7/16
	2.1	39.1	-0.518	19.1	0.427	0.426	7/8/16
Average ± s.e.m.*	**2.1±0.0**	**39.0±0.0**	**-0.455±0.047**	**19.0±0.0**		**0.435±0.006**	

ETH-3	1.6	39.4	-0.252	19.1	-0.070	0.693	10/5/15
	1.6	39.4	-0.188	19.3	0.417	0.758	3/16/16
Average ± s.e.m.*	**1.6±0.0**	**39.4±0.0**	**-0.210±0.004**	**19.3±0.0**		**0.725±0.004**	
ETH-4	-10.2	21.7	-0.294	-9.9	0.827	0.596	7/11/16
	-10.2	21.7	-0.293	-9.9	0.590	0.596	7/12/16
	-10.1	21.9	-0.283	-9.6	1.444	0.607	
Average ± s.e.m.*	**-10.2±0.0**	**21.8±0.0**	**-0.288±0.007**	**-9.8±0.0**		**0.602±0.008**	
NBS-19	1.9	38.9	-0.494	18.8	-1.762	0.450	1/21/16
	1.9	39.0	-0.498	18.8	-1.544	0.446	1/21/16
	1.9	38.9	-0.467	18.8	-2.018	0.477	1/22/16
	2.0	39.1	-0.540	18.9	-0.908	0.404	1/22/16
Average ± s.e.m.*	**2.0±0.0**	**39.0±0.0**	**-0.504±0.052**	**-18.9±0.0**		**0.441±0.052**	

Note: *s.e.m. (Standard Error of the Mean) used to estimate analytical error for samples with more than 3 measurements.
For samples with <3 measurements, standard deviation is reported.

1065

Appendix B Analytical Details

B.1 Tests on Δ_{47} clean up

Subambient and ambient (room) column temperatures were tested for optimal sample clean-up efficiency. Column performance was verified using 1000°C heated gases, CO_2 standard gases, and CO_2 derived from the acid digestion of clean (Carrara Marble) and dirty (modern non-living coral fragments; impure limestone) calcite. The column as configured above was found to clean samples effectively and provide throughput yields of CO_2 indistinguishable from 100% when processed at room temperature and allowing a 35 to 45 minute collection time, depending on sample size. Samples were analyzed isotopically within 24 hours of digestion and purification.

B.2 Corrections and Quality Control Checks on the MAT253

The analytical run structure employed a pressure baseline correction described previously. The analytical run was divided into 5 or 6 acquisitions with pressure balancing in between each acquisition to achieve a 16V signal on the 44 m/z detector. Cumulative on-peak signal integration time was generally 1000 to 1600 seconds for each of sample and reference gases, and instrumental uncertainty was at or near that calculated from counting statistics (around 10 ppm in Δ_{47}).

I performed a number of quality control checks on our analytical system. These included monitoring the Δ_{47} vs. cycle number for individual runs to ensure stable instrument performance. The 48 m/z signal was monitored for excess amplitude that would indicate inadequate cleaning of the sample gas. None of the samples used in the data chapters and models and interpretations therein gave anomalous Δ_{48} values. Nevertheless, I passed a subset of the samples through the chromatographic clean-up column a second time in order to ensure that isobaric interferences had been removed; analyses before and after the second column clean-up gave Δ_{47} values within uncertainty of each other. As a further test for isobaric interferences, I equilibrated splits of CO_2

from a few large samples at 26°C or 60°C with water, or roasted at 1000°C without water. These test equilibrations yielded Δ_{47} values that were on our equilibrated gas lines within uncertainty, indicating that sample gases were free of isobaric interferences.

B.3 Equilibrated gases and calcite standards

Tibetan samples were weighed out to yield roughly 8 to 10 mg $CaCO_3$ equivalent. Comparable size ranges of the isotopic standards NBS-18 ($\delta^{13}C$ = -5.01‰ VPDB scale; $\delta^{18}O$ = -23.20‰ VPDB), NBS-19 ($\delta^{13}C$ = 1.95‰ VPDB; $\delta^{18}O$ = -2.19‰ VPDB), and periodically LSVEC ($\delta^{13}C$ = -46.6‰ VPDB) were interspersed with the Tibetan samples.

I measured Δ_{47}, Δ_{47}, $\delta^{13}C$, and $\delta^{18}O$ relative to an Oztech (Oztech Trading Co., Safford, AZ, USA) isotopic standard gas (UOC 1766, $\delta^{13}C$ = -3.61 VPDB; $\delta^{18}O$ = 24.99 VSMOW; VSMOW used in Δ_{47} calculations) used as the working reference gas. The Δ_{47} values measured relative to the working gas were corrected to an acid digestion temperature of 25°C using the temperature dependent acid fractionation factor for calcite computed by (Guo et al., 2009). These Δ_{47} results are then converted from the working gas reference frame to the carbon dioxide equilibrium scale (Dennis et al., 2011) (CDES) using results from routine analyses of CO_2 heated to 1000°C and CO_2 equilibrated through reaction with water at 25°C and 60°C. Analyses of heated (HG) and equilibrated (EG) gases are used to generate an empirical transfer function (ETF), following the steps detailed in (He et al., 2012) and the approach of (Dennis et al., 2011). The ETF permits the conversion of Δ_{47} measurements relative to the working gas in the reference bellows ($\Delta_{47,\text{SG-WG}}$) into Δ_{47} measurements in the absolute reference frame (Dennis et al., 2011), also referred to as the "carbon dioxide equilibrium scale," and symbolized by $\Delta_{47,\text{CDES}}$. The ETF for this analytical period was $\Delta_{47,\text{CDES},25} = (\Delta_{47,\text{SG,WG}} + 1.901 \times 10^{-3} \times \delta_{47}) \times 1.00287 + 0.90941$. All data are pressure baseline (PBL) corrected (He et al., 2012).

I interspersed sample runs with digestions and analyses of reference carbonates (Table S3). These included Carrara Marble (our own sample and CM-2

from D. Schrag, Harvard University) and ETH-3 and ETH-4 (S. Bernasconi, ETH Zurich). Carrara Marble analyses, using both our sample and CM-2, are generally ca. 20-30 ppm higher in Δ_{47} than those results reported in (Dennis et al., 2011). Our ETH results are within uncertainty of the mean results from a preliminary inter-laboratory comparison reported by S. Bernasconi at the 4th and 5th International Clumped Isotope Workshops, held in August 2014, Zurich, Switzerland, and January 2016, St. Petersburg, Florida.

B.4 Error propagation and Zaarur et al. thermometer

Clumped isotope values are typically reported with either the standard error of the mean of multiple replicates of one sample or, in the case of small samples where only a single digestion is possible (n=1), the analytical error. However, when calculating a clumped isotope-derived temperature from an empirically determined Δ_{47}-T calibration, the uncertainty within the measurements used to build the calibration line must be considered. Since the development of the original Δ_{47}-T calibration (Ghosh et al., 2006a), many additional groups have reported new calibrations specific to unique carbonate materials (i.e. species-specific, cation-specific, etc.; (Henkes et al., 2013; Fernandez et al., 2014; Kele et al., 2015; Spooner et al., 2016; Winkelstern and Lohmann, 2016; Katz et al., 2017) (Fernandez et al., 2014; Henkes et al., 2013; Katz et al., 2017; Kele et al., 2015; Spooner et al., 2016; Winkelstern et al., 2016)). In addition to material type, the interlaboratory variability in slope and intercept of Δ_{47}-T calibration lines are thought to be caused by differences in lab-specific parameters such as acid digestion temperature, gas integration time (Mller et al., 2017), and choice of 17O correction (Schauer et al., 2016). However, more recent calibration studies have demonstrated that a universal Δ_{47}-T interlaboratory calibration for all material types may be possible. Fernandez et al. (2013) statistically demonstrated that importance of measuring more than the typical three replicates of each sample, more total samples, and a wider temperature calibration range to improve the uncertainty of any Δ_{47}-T calibration. For example, the Bonifacie et al. (2017) universal thermometer was calibrated over a temperature range of

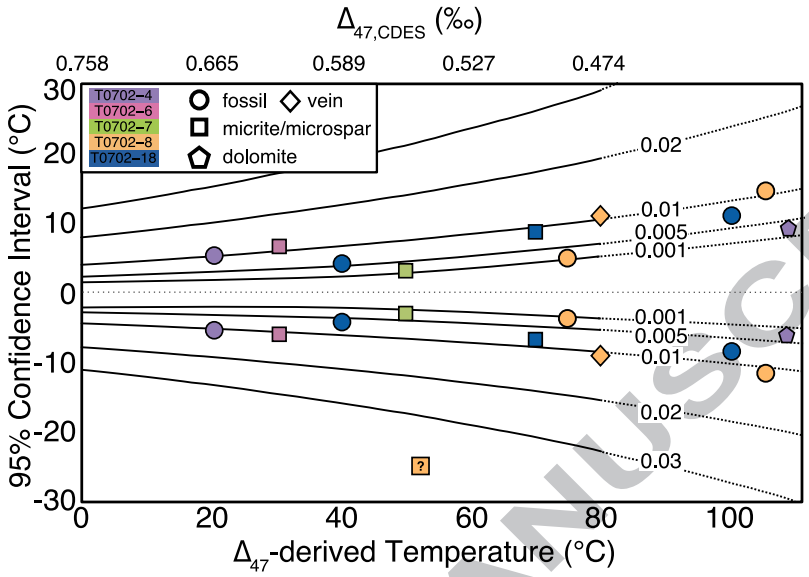

Figure S1: **95% confidence intervals of the Zaarur et al. (2013) Δ_{47} thermometer with data from this study projected based on Δ_{47}-derived temperature and analytical uncertainty.** Shapes denote the carbonate material type. Point color denotes individual samples.

25 to 350°C on 11 samples with 6 replicates, and achieved an ordinary least-squares regression slope error of 0.001. Although the OLS error of the slope of the Zaarur et al. (2013) Δ_{47}-T regression is larger (0.007) due to a narrower temperature range and fewer samples, I choose to apply this calibration to our Δ_{47}data because the analytical conditions are the most similar to the clumped isotope operation at the University of Chicago, where the data in this study were collected.

Similarly, the number of replicates of an "unknown" (i.e. a geological sample) is critical in reducing error. It is common practice to report 3 replicates of a clumped isotope measurement. However, it has been recently suggested that reporting the standard error of only a few replicates (n<10) is not statistically justifiable because when this is done, it is difficult to discern the true reproducibility of a measurement (Fernandez et al., 2017). It is more statis-

tically robust to report the mean of less than 10 replicates with a confidence interval of typically 95% or 68%. Here, I report each sample mean with 95% confidence. I determined temperature uncertainties for each measurement at the 95% confidence interval (CI) by using the statistical relationship between Δ_{47}-derived temperature and analytical uncertainty determined by Zaarur et al. (2013) for "unknown" carbonates specific to their Δ_{47}thermometer (see Fig. 2B in Zaarur et al. (2013)). Zaarur et al. (2013) used an inverse-regression method to calculate the relationship between the temperature calibration and prediction uncertainties. The precision of the calibration alone at the data centroid (27°C) used to construct the contours in Fig. S1 is ±2°C. The majority of the Tso Jianding carbonates have a 95% CI of <10°C using the Zaarur et al. (2013) calibration. An outlier, T0706-8 (box with question mark in Fig. S1), represents three individual digestions of carbonate drilled from one location on the cut sample surface. The temperature uncertainty within 95% CI is greater than that modeled by Zaarur et al. (2013), and therefore the point was projected to the best of our ability. While the T0702-8 microspar is not useful in reconstructing a primary or even secondary carbonate crystallization temperature, I am able to use the analytical irreproducibility to make an assessment of the extent of alteration this rock has experienced. A mean Δ_{47} value of $52^{+30}/_{-25}$°C suggests that T0702-8 is an admixture of a multi-component carbonate system within the small hand sample, and therefore multiple generations of carbonate alteration and potentially stable mineral recrystallization occurred during this rocks burial history.